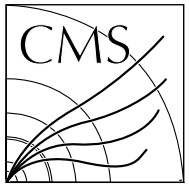

The Compact Muon Solenoid Experiment

CMS Note

Mailing address: CMS CERN, CH-1211 GENEVA 23, Switzerland

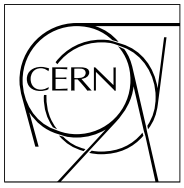

April 2006

Detection of New Heavy Charged Gauge Bosons in the Muon plus Neutrino Channel

C. Hof, T. Hebbeker, K. Hoepfner

RWTH Aachen, III. Phys. Inst. A, Germany

Abstract

This note presents the first feasibility study [1] of the search for a new heavy charged gauge boson with the CMS detector at the Large Hadron Collider LHC. The model assumes the existence of a heavy carbon copy of the Standard Model W (Reference Model by Altarelli) generically denoted as W'. Such a boson has been investigated in the decay channel $W' \rightarrow \mu\nu$ using the full detector simulation including minimum bias events (pile-up) according to the expected first years of luminosity. All relevant Standard Model backgrounds have been considered.
Such a new boson is expected to be discovered, if existing, with a mass up to 4.6 TeV for an integrated luminosity of 10 fb^{-1}. The range can be expanded to 6.1 TeV with an integrated luminosity of 300 fb^{-1}. If no signs for a W' boson appear 95% CL exclusion limits of 4.7 TeV and 6.2 TeV can be set respectively.

1 Introduction

Several theories beyond the Standard Model (SM) introduce new charged gauge bosons in order to enlighten phenomena which cannot be explained in the context of the Standard Model. For example Left-Right Symmetric Models (LRSM) restore parity at high energies by predicting an additional heavy charged gauge boson called W' and explain parity violation at low energies by the difference of the W and W' masses.

In principle every expansion of the Standard Model gauge groups leads to new gauge bosons, which are related to the generators of the new symmetry. Therefore a huge variety of models demanding new gauge bosons exists. So far, only the Standard Model bosons (γ, W, Z and the gluons) have been discovered and hence new charged particles are expected to have masses at the TeV scale. The decay of such bosons into high energy final state particles induce prominent signatures for physics beyond the Standard Model.

In this paper, a study of a W' boson decaying into a single muon and a neutrino is presented. We do not assume any special extended gauge theory. Instead the investigated W' boson is based on the Altarelli Reference Model [7]. It treats the W' boson as a massive carbon copy of the Standard Model W with branching ratios and a cross section comparable to extended gauge theories such as LRSM. The resulting experimental signature of a high energy muon accompanied by a large amount of missing energy allows an easy separation of signal and background events using the transverse invariant mass (see below).

In order to determine the detection probability as a function of the W' mass a statistical method ($\mathrm{CL_S}$-method) is applied to the transverse invariant mass spectrum of the W' signal and the expected SM background.

2 Theories covering W' Bosons

Some of the models introducing W' bosons, which can be addressed at the LHC, and especially the one used for this search, are briefly reviewed.

2.1 Left-Right Symmetric Models

Within the Standard Model the origin of parity violation within weak interactions stays unexplained. The Standard Model multiplets of particles are explicitly designed to break parity in the weak sector to match the experimental observations: the left-handed particles are assigned to doublets, whereas the right-handed particles are $\mathrm{SU(2)_L}$ singlets and thus do not participate in weak interactions via charged currents.

Left-Right Symmetric Models [2–6] address this remedy and provide an attractive extension of the Standard Model. The general feature of these models is the intrinsic exact parity symmetry of the Lagrangian through an additional $SU(2)$ gauge group, resulting in an observable W' (and Z' respectively). The according gauge group of the electroweak sector is therefore

$$SU(2)_{\mathrm{L}} \times SU(2)_{\mathrm{R}} \times U(1)_{\mathrm{B\text{-}L}}. \tag{1}$$

The SM fermion doublets are mirrored by arranging the right-handed singlets of the Standard Model together to form another $SU(2)$ doublet. In the lepton sector this can only be done by predicting a neutrino singlet ν_{R} for each generation, which is a massive Majorana particle

$$u_{\mathrm{R}}, d_{\mathrm{R}} \rightarrow \begin{pmatrix} u_{\mathrm{R}} \\ d_{\mathrm{R}} \end{pmatrix}; \qquad \nu_{\mathrm{R}}, l_{\mathrm{R}} \rightarrow \begin{pmatrix} \nu_{\mathrm{R}} \\ l_{\mathrm{R}} \end{pmatrix}. \tag{2}$$

Both doublets cannot be assigned to the same SU(2) gauge group, since this would result in a vector current instead of the observed V$-$A current in weak interactions. Because of the right-handedness of the fermions the group $SU(2)_{\mathrm{R}}$ is indexed by an “R”.
To match the low-energy behaviour of maximum parity violation in weak interactions, the symmetry is spontaneously broken by a scalar Higgs field. In addition, LRSMs incorporate full quark-lepton symmetry and turn the quantum number of the U(1) from hypercharge Y to the value of baryon-minus-lepton number B$-$L. Finally, in choosing an appropriate Higgs sector, the theory gives a natural explanation for the smallness of the neutrino masses by relating it to the observed suppression of V + A currents.

2.2 Other Models with Additional Bosons

Left-Right Symmetry can be embedded in models with larger gauge symmetry groups such as $SO(10)$. Within these models they occur as an intermediate state of a symmetry breaking pattern. Thus, the variety of such models is in principle arbitrary large [8]: they range from Grand Unified Theories over Supersymmety to Extra Dimensions. Little Higgs Models, being in the actual focus of some theorists, should be mentioned here as an alternative theory predicting a W' boson at energies of the LHC.

Little Higgs Models

Little Higgs Models provide a new formulation of the physics of electroweak symmetry breaking. The key features of those models are summarized here (for details see [9]):

- The Higgs fields are Goldstone bosons, which are associated with some global symmetry breaking at a higher scale.
- The Higgs fields acquire mass and become pseudo Goldstone bosons via symmetry breaking at the electroweak scale.
- The Higgs fields remain light since they are protected by the global symmetry and are free from a 1-loop quadratic sensitivity to the cutoff scale up to which the theory is valid.

In addition to the Standard Model gauge bosons, a set of heavy gauge bosons are included in Little Higgs Models having the same quantum numbers as the massive SM gauge bosons. By the choice of the gauge coupling constants, the Higgs bosons quadratic divergences, induced by SM gauge boson loops, are canceled by quadratic divergences of the new heavy gauge bosons.
These new particles are expected to appear at the TeV-scale and should be detected at the LHC if they exist. Moreover, the entire reasonable parameter space of Little Higgs Models can already be investigated with one year of LHC data [10].

2.3 The Reference Model

Because of the variety of models with their special assumptions, we do not consider one of the models mentioned above, but investigate the detection capabilities for a hypothetical heavy partner of the Standard Model W. Its properties are derived in a more general framework from the Reference Model by Altarelli [7].

The Model is obtained by simply introducing ad hoc new heavy gauge bosons, two charged W' vector bosons as well as one neutral Z' boson, as carbon copies of the Standard Model ones. Additional neutrinos are not taken into account within the model. The couplings are chosen to be the same as for the ordinary W and Z bosons. The only parameters are the masses of the new vector bosons. While the coupling of the so constructed bosons to leptons is comparable to those obtained in extended gauge theories, the couplings to the massive Standard Model gauge bosons are enlarged [7]. For W' masses larger than 500 GeV this leads to a W' width larger than its mass. Since such a state is not interpreted as a particle any more, the couplings of W' and Z' bosons to the Standard Model W and Z are suppressed manually in the Reference Model. This results in a moderate width for the new gauge bosons.

Such a suppression arises in a natural manner in extended gauge theories: if the new gauge bosons and the SM ones belong to different gauge groups, vertices of the kind $Z'ZZ$ or $W'WZ$ are forbidden. They can only occur after symmetry breaking due to mixing of the gauge group eigenstates to mass eigenstates. These vertices are then suppressed by a factor of the order of $(m_{\mathrm{w}}/m_{W'})^2$. With these assumptions the Reference Model has branching ratios (see table 1), cross section and width (see figure 1) comparable to extended gauge theories. Thus it is a reasonable approach for a direct search.

Due to the variety of theories covering W' bosons, this model has been used in serveral earlier experiments, so that the resulting limits given in this study can be compared easily. Previous searches for Reference W' at LEP and the Tevatron exclude such bosons with a mass up to 1 TeV [11] (for a review of W' mass limits using different models see [12]).

Branching Ratios						
Model	Reference Model			LRSM (M_{ν_R} = 0.5 TeV)		
$M_{W'}$	1 TeV	2 TeV	5 TeV	1 TeV	2 TeV	5 TeV
$W'^{+} \to \bar{d}u$	24.2%	24.0%	23.9%	26.7%	24.6%	24.0%
$W'^{+} \to \bar{d}c$	1.2%	1.2%	1.2%	1.4%	1.3%	1.2%
$W'^{+} \to \bar{d}t$	0.0%	0.0%	0.0%	0.0%	0.0%	0.0%
$W'^{+} \to \bar{s}u$	1.2%	1.2%	1.2%	1.4%	1.3%	1.0%
$W'^{+} \to \bar{s}c$	24.2%	24.0%	23.9%	26.6%	24.5%	24.0%
$W'^{+} \to \bar{s}t$	0.0%	0.0%	0.0%	0.0%	0.0%	0.0%
$W'^{+} \to \bar{b}u$	0.0%	0.0%	0.0%	0.0%	0.0%	0.0%
$W'^{+} \to \bar{b}c$	0.0%	0.0%	0.0%	0.0%	0.0%	0.0%
$W'^{+} \to \bar{b}t$	24.3%	25.0%	25.1%	26.7%	25.5%	25.1%
$W'^{+} \to l^{+}\,\nu_{l_{(R)}}$	8.2%	8.2%	8.2%	5.7%	7.6%	8.1%

Table 1: Comparison of the branching ratios of the W' boson in a Left-Right Symmetric Model and the Reference Model for different masses obtained by PYTHIA [13]. The mass of the massive Majorana neutrino in the LRSM is set to 500 GeV. For W' masses much larger than the Majorana neutrino mass the leptonic branching ratios are almost identical.

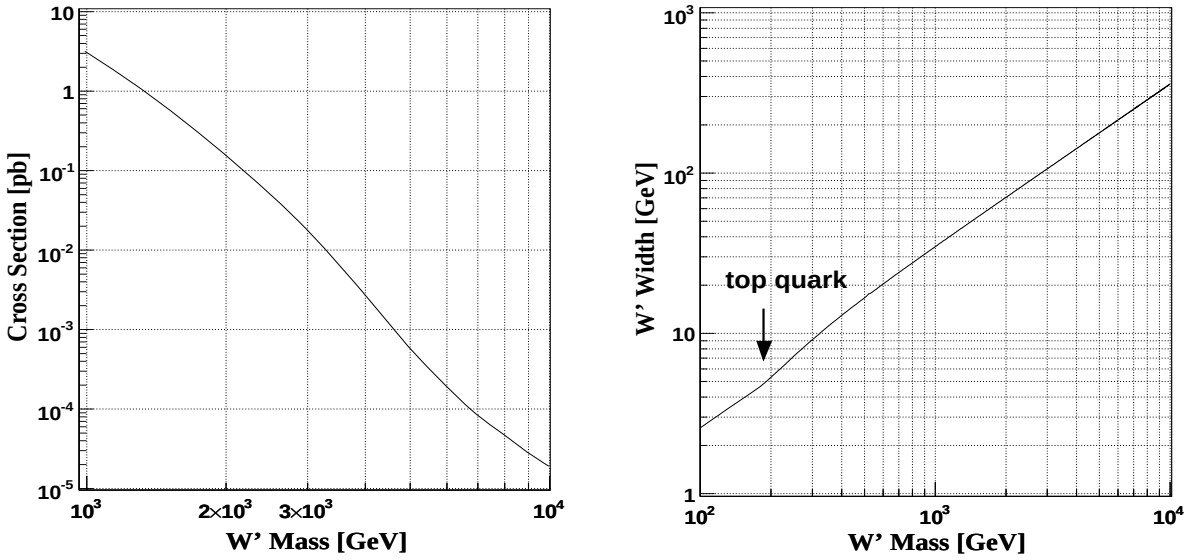

Figure 1: The cross section (left) and the width of the W' boson as a function of its mass obtained by PYTHIA. The small kink in the width at around 200 GeV results in the additional decay channel of the W' boson into a top and bottom quark, which is kinematically not allowed for the SM W.

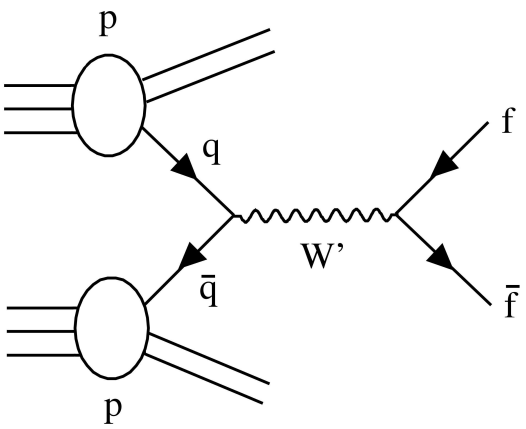

Figure 2: Feynman graph of the W' boson production at leading order. A quark-antiquark pair annihilates into a W' boson and decays into a fermion pair.

3 Detection of Muons and Missing Energy in CMS

CMS [14] is a multi-purpose detector with a high resolution silicon tracker, a $PbWO_4$ electromagnetic calorimeter along with a sandwich hadronic calorimeter and a complex muon system. The detection of the decay $W' \to \mu\nu$ relies on the identification capabilities of the muon system and the ability to infer the occurance of the neutrino from the determination of missing transverse energy.

The CMS muon system [15] is interleaved with the iron return yoke needed for the 4 T coil and consists of three detection subsystems: drift-tube chambers (DT) in the barrel part ($|\eta| < 1.2$), cathode strip chambers (CSC) in the two end-caps ($1.2 < |\eta| < 2.4$) and resistive plate chambers (RPC) in both barrel and end-caps (see figure 4). A muon originating from the nominal pp interaction point crosses up to four muon stations.

Each drift tube chamber in the barrel contains 3×4 layers of staggered drift cells, where 2×4 layers measure the bending of the muon trajectory in the r,ϕ-plane of CMS while one group of 4 layers determines the coordinate perpendicular to it (θ view). The only exception of this scheme are the outermost chambers consisting of only two superlayers in the r,ϕ-plane. The basic detection element of a drift tube chamber is a 42×13 mm drift cell, flushed with a gas mixture of 85% Ar and 15% CO_2.

The cathode strip chambers in both end-caps are multi-wire proportional chambers (40% Ar, 50% CO_2, 10% CF_4) with six individual layers of anode wires and segmented cathodes. The strips inside the trapezoidal chambers are oriented radially with the wires perpendicular to them. Strips measure the muon position in the azimuthal ϕ direction and wires provide, less precisely but with faster response, the radial position. The fast wire information is primarily used for the trigger but supports also the coordinate reconstruction The high spatial precision is provided by the cathode information.

The resistive plate chamber system is complementary to the other muon detectors. Its excellent time resolution of a few nanoseconds is specifically designed for trigger purposes and adds robustness and redundancy to the muon system.

The CMS trigger system has two physical levels. The first level (L1) is implemented on custom-built hardware while the second level (HLT) is based on software. The first level global trigger has to decide every 25 ns whether to accept or reject the event based on coarse information from the calorimeter and the muon system (Global Muon Trigger).

The Global Muon Trigger may use information from all three complementary subsystems - the fast RPC timing information, the regional CSC and regional DT trigger - with the goal of reconstructing position and momentum of muons and assigning a bunch crossing with high efficiency.

The L1 muon trigger for DT and CSC works in several consecutive steps. First, the information of each chamber is processed independently by on-chamber local trigger electronics to reconstruct track segments at the chamber level. The individual segments are matched by higher level trigger electronics into a single muon candidate, assigning the track parameters p_{T}, η, ϕ and quality. The Global Muon Trigger matches the muon candidates from the DT and CSC Track Finder with the RPC information in order to choose the four best muon candidates with the highest transverse momentum p_{T}.

The CMS tracker provides up to 10 measurements of the track trajectory using silicon strip detectors. The muon momentum is measured with a high resolution through bending in a 4 T magnetic field. To fully reconstruct the muon, the information of the silicon tracker is combined with measurements of the muon system. The tracker dominates the momentum resolution for muon momenta up to $\sim$200 GeV due to the fact that multiple scattering in the iron return yoke limits the stand-alone momentum resolution of the muon system. A fully reconstructed muon based on tracker and muon information is called a "Global Reconstructed Muon" to be distinct from "Local Reconstructed Muons" in either subsystem.

The neutrino, the other decay product of a W' boson, cannot be detected directly but has to be infered from the observation of missing energy, provided by the calorimeters, in particular the hadronic calorimeter. In addition the momentum carried away by the muons has to be taken into account, since they are not stopped within the calorimeter.
CMS operates a standard sandwich calorimeter. The active elements are scintillator panels which generate photons when charged particles pass through, a small fraction of which is read out by photon detectors.
The hermetic calorimeters cover a range up to $|\eta| = 5$ so that a significant amount of the collding particles escapes through the beam pipe. Therefore the detection of the neutrino is only possible within the transverse plane as missing transverse energy $\not{E}_{\mathrm{T}}$.

4 Signal and Background Simulation and Reconstruction

4.1 The Signal

Given that the W' boson is a massive object, it is likely to be produced without transverse momentum. The decay energy of the W' boson is shared among the muon and the neutrino being emitted back-to-back in the W' boson rest frame (see figure 4). Due to a boost along the z-axis, the angle between the muon and the neutrino might be different from 180° in the laboratory system. However, the angle in the transverse plane stays invariant under boosts along the z-axis.
At hadron machines events containing neutrinos suffer from a general problem: neutrinos are only indirectly detectable as an energy imbalance, which can only be determined in the transverse plane, since a sufficient amount of energy is taken away through the beam pipe. Therefore the analysis of a W' boson decaying into a lepton and a neutrino is generally restricted to a plane perpendicular to the beam line.

Beside the muon and the missing transverse energy from the $W' \rightarrow \mu\nu$ decay, underlying events result from the same or multiple pp-collisions. Along with additional particles from the same und further collisions, they may cause pile-up events. Therefore a $W' \rightarrow \mu\nu$ event has the "clean" signature of a high energy isolated muon, together with a large amount of missing energy pointing into the opposite direction in the transverse detector plane. Due to the small transverse momentum of the W' boson, the transverse momentum of the muon and the missing transverse energy are of similar magnitude.

The signal data samples have been generated using the full CMS detector simulation and event reconstruction software including an average of 3.5 pile-up events per signal event, corresponding to the low LHC luminosity phase ($\mathcal{L} = 2 \cdot 10^{33}\ \mathrm{cm}^{-2}\,\mathrm{s}^{-1}$). As an input to the full detector simulation W' events based on Altarelli's Reference Model (see section 2.3) have been generated at leading order (see figure 2). The only parameter within this model is the mass of the W' boson. Since the current lower mass bound on the W' boson is slightly below 1 TeV the first sample is generated with this mass. Further samples follow with masses of 2–8 TeV. The upper limit is given by the W' production rate, which is less than one event in 10 fb^{-1} for W' masses larger than 7 TeV. In total about 300.000 events have been produced (see table 2). The product of LO cross section and branching fraction varies between 3.0·10^{3} fb (1 TeV) and 3.3·10^{-4} fb (8 TeV), to be compared to 1.7·10^{7} fb for Standard Model W production and muonic decay.

4.2 The Background

Relevant backgrounds are qualified by a very similar signature compared to the signal. From figure 3 one obtains that muons with transverse momenta larger than 30 GeV are mostly resulting from the decay of gauge bosons, in particular W. Since the massive charged SM gauge bosons decay in the same manner as the W' boson, they have identical signatures. However, due to the huge mass difference of the W and the W' (> 1 TeV) the transverse momentum of the muon and the transverse missing energy originating from the SM W are much smaller.

Other sources of high energy muons are the decays of heavy quarks. They hadronize and may produce mesons, which also decay into muons (*e.g.* b-quarks). Since these muons are accompanied by a jet and thus are not isolated,

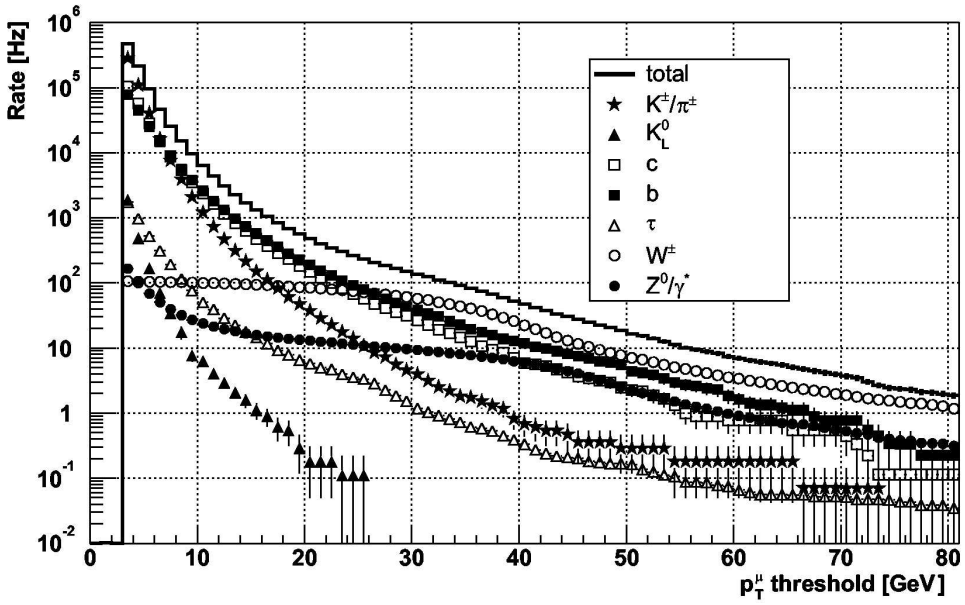

Figure 3: Inclusive single muon production rate as a function of the muon p_{T}-threshold at the LHC with a luminosity of $\mathcal{L} = 10^{34}\ \mathrm{cm}^{-2}\,\mathrm{s}^{-1}$. The plot is generated using PYTHIA with a restricted acceptance $|\eta| < 2.1$ [16].

they can be rather easily identified as background. Among the quarks the top quark is an exception. It decays nearly always into a W and a b-quark and therefore top-antitop events are also taken into account for this analysis.

Based on these facts, the backgrounds have been determined to be

- **single W-production** with a subsequent decay into a muon and a neutrino,
- **single Z-production**, decaying into two muons,
- **gauge boson pair production WW, WZ and ZZ,**
- **$t\bar{t}$ pair production,**
- **QCD**.

The analysed data samples, which have been produced within the Data Challenge 2004 are listed with the corresponding cross sections and number of events in table 2. Due to the restricted computing power and the long time which is necessary for the production of one event, the number of simulated events is limited. To reduce the needed computing time acceptance cuts are applied already at the generator level (PYTHIA). This is mainly important for processes with a large cross section like single W- or Z-production, where such constraints save the simulation of several 10^5 events.

For the $W \rightarrow \mu\nu$ sample the event is only fully simulated, if the muon has a transverse momentum larger than 14 GeV and penetrates the detector with angles corresponding to $|\eta| < 2.5$. This is sensible since the muon system only covers an area up to $|\eta|$ = 2.4. The muons in the $Z \rightarrow \mu\mu$ sample are also constrained to $|\eta| < 2.5$ and must have transverse momenta larger than 20 GeV and 10 GeV, respectively, to pass the generator level. In addition the invariant mass of the muon pair must be larger than 10 GeV.

No constraints are applied to the pair boson samples WW, WZ, ZZ and the $t\bar{t}$ sample. A different approach has been taken for the generation of the so called "QCD"-events. This synonym covers (at leading order) events of the type $qq \rightarrow qq$, $q\overline{q} \rightarrow q\overline{q}$, $q\overline{q} \rightarrow gg$, $qg \rightarrow qg$, $gg \rightarrow q\overline{q}$ and $gg \rightarrow gg$. Since these kinds of processes, especially those with a low momentum transfer of the partons, dominate by far at hadron colliders, the QCD-events have been produced in various disjunct samples. The events are separately simulated for different values of the transverse momenta $\widehat{p}_{\mathrm{T}}$ of the final state partons in their rest frame.
For this study the QCD samples have been analysed separately, scaled according to the cross section and finally merged into one sample.

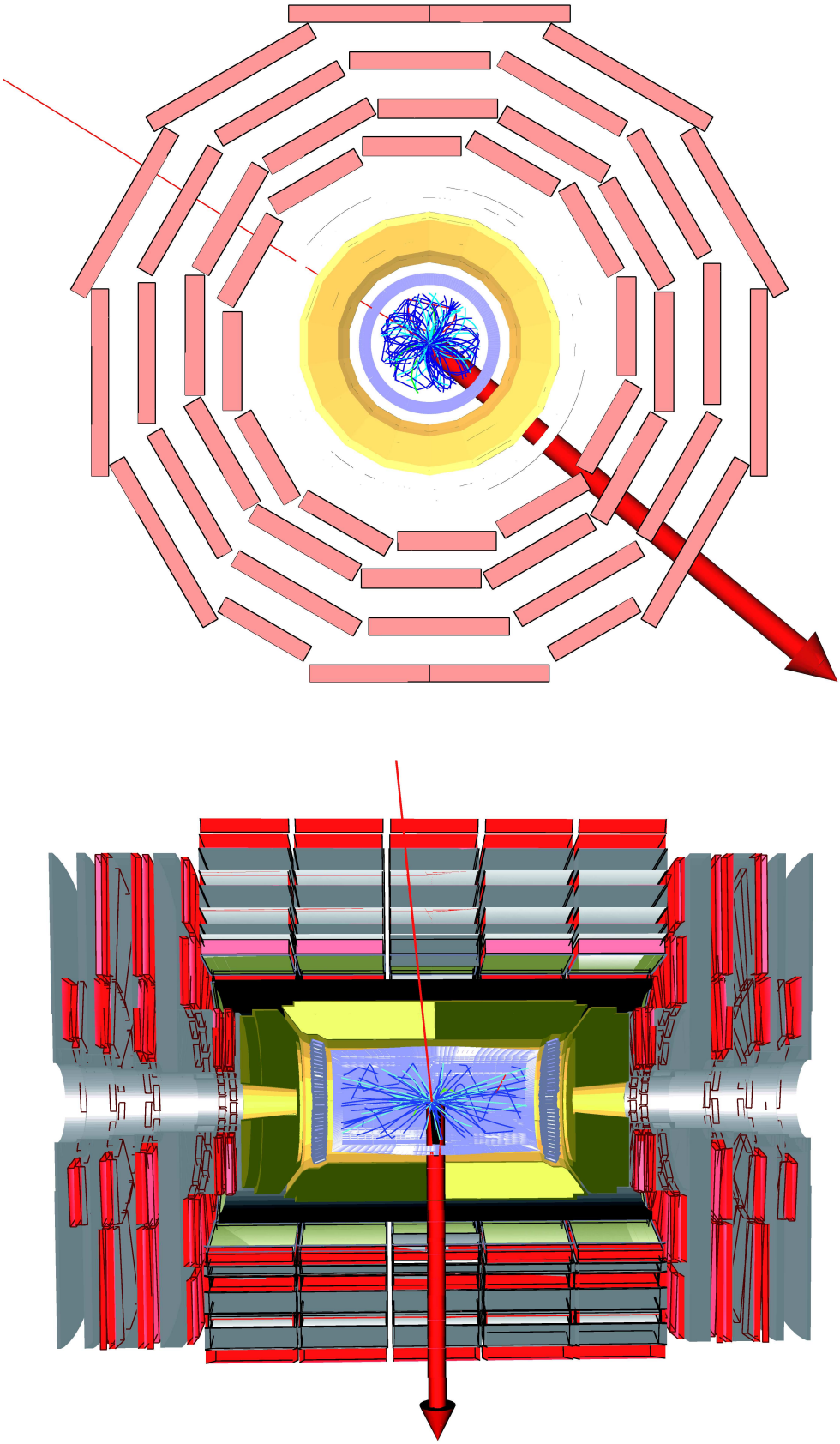

Figure 4: A 1 TeV W' boson event displayed by the CMS event display. In the transverse (top) and longitudinal plane (bottom) the muon (thin red line) and the missing transverse energy (thick arrow) are shown. Further tracks are visible in the tracker coming from underlying events and pile-up as explained in the text.

4.3 Speciality of the W Background

These studies have shown that the main source for background to the W' signal are W bosons, which arise within several reactions like $t\bar{t}$, single W or double boson production (WW, WZ, ZZ). These bosons give rise to background in three different ways:

1. W bosons which are produced offshell may have a mass comparable to a W' boson. These offshell produced bosons cannot be distinguished from a W' and therefore represent an irreducible W' background. However, the cross section for offshell production is expected to be below the W' cross section for the reviewed W' masses.

2. Since the W boson cross section is of the order of 10^7 times larger than the W' boson cross section, poorly reconstructed muons and/or missing energy might fake W' bosons. By demanding a high precision reconstruction especially of the muons this reducible background is minimized. Therefore a high precision muon reconstruction is essential for this analysis and cuts have been developed to improve the default precision.

3. W bosons with large transverse momenta arising from the recoil against a jet result in muons with larger momentum or a larger amount of missing energy compared to a W decaying at rest. Since the transverse invariant mass is used within this W' search, W bosons with large p_{T} can be excluded as background in the ideal case of perfect muon and missing energy reconstruction.

The background samples mentioned above do not cover the total range of the signal's transverse invariant mass. To perform a detailed statistical analysis, it is necessary to generate background events with high transverse momenta comparable to those obtained from a W' decay. Since the $W \to \mu\nu$ dominates the background after performing selection cuts (see below), further W samples have been produced choosing special ranges for the transverse momentum $\widehat{p}_{\mathrm{T}}$ of the muon and neutrino in the rest frame of the W. 200 events each have been produced in 50 GeV-steps in the $\widehat{p}_{\mathrm{T}}$-range from 200–500 GeV and 100 GeV-steps from 500–3000 GeV.

Background			
Type	Cross Section [fb]	Analysed Events	Remark
$W \to \mu\nu$	$1.72{\cdot}10^{7}$	1484000	
$W \to \mu\nu$	$1.48{\cdot}10^{2}$	200	$200\ \mathrm{GeV} < \widehat{p}_{\mathrm{T}} < 250\ \mathrm{GeV}$
$W \to \mu\nu$	$4.05{\cdot}10^{0}$	200	$450\ \mathrm{GeV} < \widehat{p}_{\mathrm{T}} < 500\ \mathrm{GeV}$
$W \to \mu\nu$	$1.90{\cdot}10^{-1}$	200	$900\ \mathrm{GeV} < \widehat{p}_{\mathrm{T}} < 1000\ \mathrm{GeV}$
$W \to \mu\nu$	$9.32{\cdot}10^{-4}$	200	$1900\ \mathrm{GeV} < \widehat{p}_{\mathrm{T}} < 2000\ \mathrm{GeV}$
$W \to \mu\nu$	$7.76{\cdot}10^{-6}$	200	$2900\ \mathrm{GeV} < \widehat{p}_{\mathrm{T}} < 3000\ \mathrm{GeV}$
Z inclusive	$1.45{\cdot}10^{8}$	720000	
WW inclusive	$1.88{\cdot}10^{5}$	480000	
ZZ inclusive	$1.11{\cdot}10^{4}$	480000	
ZW inclusive	$2.69{\cdot}10^{4}$	280000	
$t\bar{t}$ inclusive	$4.92{\cdot}10^{5}$	2300000	
QCD	$> 6{\cdot}10^{8}$	$>$ 2000000	
Signal			
W' (1 TeV) $\to \mu\nu$	$3.01{\cdot}10^{3}$	45000	
W' (2 TeV) $\to \mu\nu$	$1.49{\cdot}10^{2}$	8400	
W' (3 TeV) $\to \mu\nu$	$1.61{\cdot}10^{1}$	8200	
W' (4 TeV) $\to \mu\nu$	$2.06{\cdot}10^{0}$	7200	
W' (5 TeV) $\to \mu\nu$	$2.73{\cdot}10^{-1}$	4400	
W' (6 TeV) $\to \mu\nu$	$3.38{\cdot}10^{-2}$	900	
W' (7 TeV) $\to \mu\nu$	$3.70{\cdot}10^{-3}$	250	

Table 2: The simulated data samples used in this study (not all signal samples are listed). The cross section (times branching ratio) obtained from PYTHIA at leading order using the parton density function CTEQ 5L (leading order) and the number of analysed events (before applying any cuts) are given. As mentioned in the text different $W \to \mu\nu$ samples have been used within this study: one sample with transverse invariant masses at the order of the W mass and additional samples with invariant masses at the order of the W' mass. For the latter samples exemplary some cross sections are listed.

The various additional samples can be easily scaled according to their luminosity and merged into one sample, since they have been produced in disjunct $\widehat{p}_{\mathrm{T}}$-ranges. But the sample, which has been produced without any constraints on $\widehat{p}_{\mathrm{T}}$, has some "overlap" with the additional produced ones. To avoid "double-counting" of W events the "overlap"-region has been identified within the $\widehat{p}_{\mathrm{T}}$-distribution. In this region a cut has been applied to make one sample end at the cut, while the other starts at this point.

5 Event Selection

In order to extract a clear W' boson signal, prior hidden by Standard Model background, selection criteria are applied to the simulated data. The selection process results in a final variable with an improved signal to background ratio. Since the transverse invariant mass combines all available information from the leptonic decay of a W' boson the observation significance is determined by using this variable. In figure 5 the final variable for signal and background is shown before applying any cuts.

In this chapter, both, the simulated signal and the simulated Standard Model background are presented as well as the cuts used to enrich the relative signal contribution within the final variable[1)].

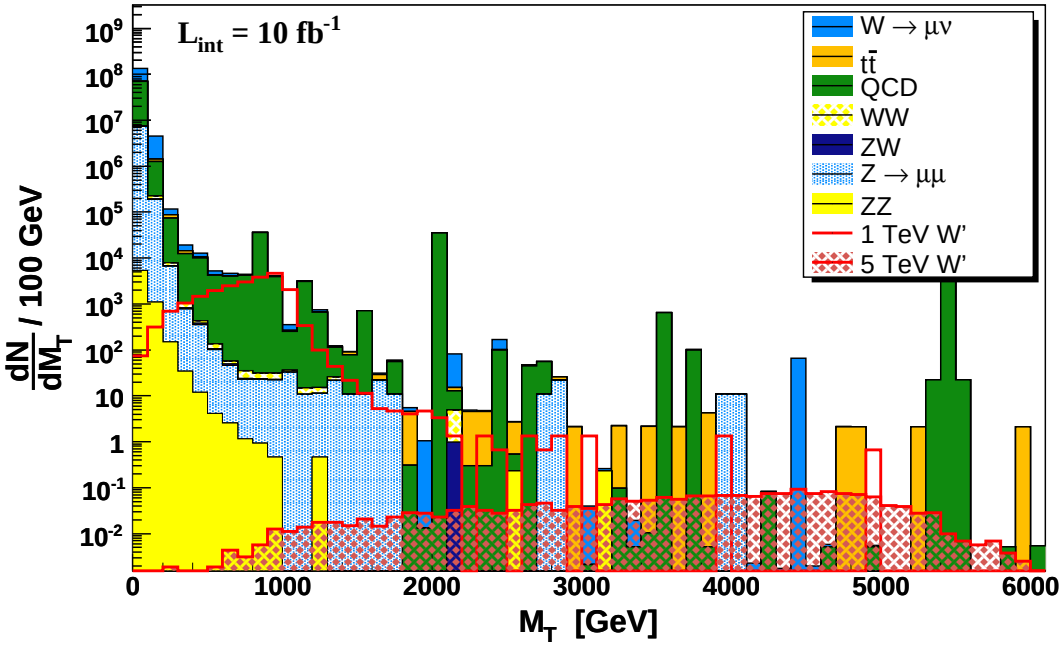

Figure 5: Distribution of the transverse invariant mass without applying any cuts for the signal and SM background. The 1 TeV and 5 TeV W' signal (non-stacked) and the background (stacked) for an integrated luminosity of 10 fb^{-1} are drawn. For each event the highest energy muon and the missing transverse energy are combined to obtain the transverse invariant mass. Over the whole range the background (mainly QCD) is even larger than the 1 TeV W' signal.

5.1 Preselection

Before starting with the analysis, the MC events have to pass preselection criteria, mainly to sort out events which are not accepted by the Level-1 Trigger. Such events are reconstructed in the full detector simulation, but an identical event in a running CMS detector would not be written on tape.
Events which enter this analysis

- have to contain at least one Global Reconstructed Muon,
- have to pass the Level-1 Single Muon Trigger
- and the High Level Trigger.

[1)] In all of the shown plots the signal is *not* added to the background ("non-stacked"), but drawn in front of it.

The first criterion naturally arises from the fact that the signal significance is determined using the transverse invariant mass calculated from the transverse momentum of the muon and missing transverse energy. The use of Global Reconstructed Muons also demands a quality standard for the reconstructed object as documented in [17]. The latter two constraints ensure that the event will be recorded by a fully operational CMS detector.

Since the detector simulation uses the start-up detector geometry, the CSCs close to the beam pipe (ME1/1) have only a limited readout. It implies that the single muon trigger is less efficient in the range $|\eta| > 2.1$.
The so defined starting sample is now investigated for criteria, which allow a distinction between signal and background. The cuts applied for this purpose are stated and explained in the following.

5.2 Selection Criteria

After the preselection, cuts have been applied to the data in order to suppress background and to improve the signal to background ratio within the final variable. According to the $W' \to \mu\nu$ signature the following cuts have been applied:

- **Muon Quality**
  Since a muon, which is reconstructed only from a few hits or which results from a poor track fit might fake a high energy muon, cuts are applied to the muons to ensure a high quality reconstruction.
- **Single Muon Requirement**
  In contrast to Z bosons, which decay into muons, $W' \to \mu\nu$ events give rise only to a single muon. Especially to suppress the background from neutral gauge bosons, events with more than one muon are excluded from the final variable.
- **Muon Isolation**
  Muons arising from decaying gauge bosons are isolated. An isolation criterion reduces the background from non-isolated muons, which originate within a particle jet (*e.g.* QCD).

A detailed motivation and explanation of the different cuts are given in the following subsections.

5.2.1 Muon Quality

The rate of low energy muons arising from different SM backgrounds is several orders of magnitude larger than the rate of high energy muons from W' bosons. Assuming that every 10^5th low energy muon is wrongly reconstructed as a high energy one, the high-p_{T} muon rate would be dominated by these muons. The observation of a W' signal within this "background" would be impossible. Therefore a high quality reconstruction of muons in the full transverse momentum range of 5–4000 GeV is essential for the detection of a possible W' boson at the LHC.

Within this study it has turned out that the quality of the muons can be improved by demanding criteria, in addition to the ones applied by the reconstruction software. They are based on the number of hits (degrees of freedom), which are used for the muon's track fit and the deviation of the muon track from the single hits, namely the χ^2-value of the track fit.

Degrees of Freedom for the Muon Track

This quality cut takes into account that the properties of particles which are measured at a multitude of points along a large distance can be determined very precisely. Inverting this statement the properties of a particle measured at only a few points have on average larger errors and might vastly differ from the actual properties. Therefore only muons which are measured at a certain number of points enter the final variable.

This analysis aims for high energy muons especially with transverse momenta larger than 200 GeV. Due to the high penetration power muons are normally not stopped within the detector. Under the assumption that the muons pass at least two muon stations, their tracks should be visible also inside the pixel detector and the silicon tracker. This results in a minimum of 10 measurements inside the inner tracker (2–3 within the pixel detector and at least 7–8 inside the tracker). Adding further track information from two muon stations with their RPCs results in at least 15 overall track measurements. Since these measurements always consist of two coordinates a track fit is constrained by 15·2 = 30 "single" measurements.

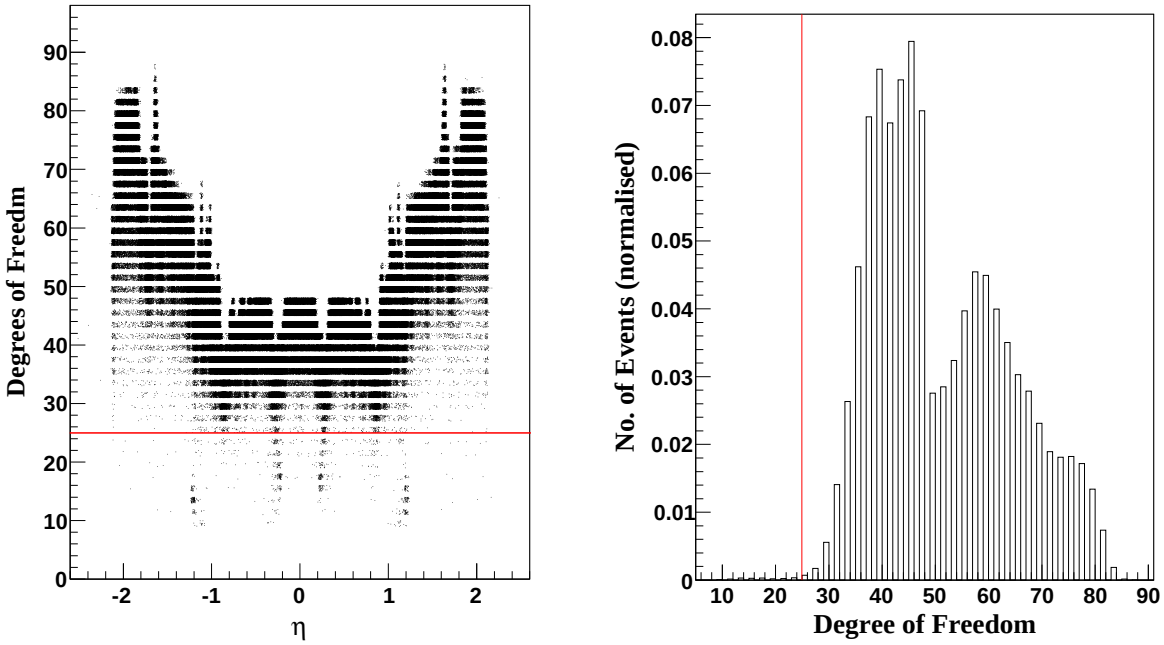

Figure 6: The muon degrees of freedom (= number of used measurements minus five fit parameters) as a function of η (left) and the overall distribution (right) are shown for the $W \to \mu\nu$ sample. All other cuts have been applied.

In general, a track is fitted with five parameters (for details see [18]). An equation with 5 parameters constrained by 30 measurement results in 25 degrees of freedom for the track fit. This is the minimum number of degrees of freedom required for a high quality muon to be used in this study.

Figure 6 displays the distribution of the number of degrees of freedom as a function of the pseudorapidity η for the muons in the $W \to \mu\nu$ sample. The structure of the muon system (barrel wheels and endcap discs) is clearly visible. The transition regions, which are not fully covered by active detector volumes, show cracks in the acceptance. A major part of these muons, crossing the less instrumented detector areas, are excluded by this quality cut. This is a crucial cut since the reconstruction of muons with a small number of measurements is more error-prone and might fake a high-p_{T} muon. As obtained from figure 6 only a small fraction of simulated muons do not pass this quality criterion (compare with table 3 and 4).

χ^2-Criterion for Muon Track

A high quality track fit is characterised by a small deviation of the fitted track from the used measurements. The χ^2-value of the fit is a quality criterion for the reconstructed track. However, a small χ^2-value does not guarantee a good fit: a fit through only a few measurement points has naturally a smaller χ^2-value than an extrapolation using a larger number of hits. The χ^2 normalised to the degrees of freedom of the muon track remedies this drawback. The value can be interpreted as a kind of mean deviation per measurement and thus provides a reasonable quality measurement.

Such distributions for the $W \to \mu\nu$ sample and the 1 TeV W' boson sample are displayed in figure 7. They are characterised by an accumulation of nearly all the muon tracks at low values and a large tail giving rise to values up to 400. A sensible value for the separation of these two areas is χ^2 divided by the degrees of freedom of 50 (see figure 7). This cut has therefore been chosen to further increase the quality of the reconstructed muons. The choice is confirmed by the comparison of the reconstructed muon p_{T} with the generator input (see figure 8): the relative error of the excluded muons is significantly larger. Especially those muons, which have a large p_{T}-deviation, are sorted out.

An exact separation of well reconstructed muons from badly reconstructed ones or even fakes is not possible with this cut. However this criterion is a compromise between quality assurance and signal efficiency. Smaller values (down to 10) for this cut have been tried without any reduction of non-Gausian tails within the transverse momentum resolution. Therefore only the tail of the χ^2-distribution has been excluded.

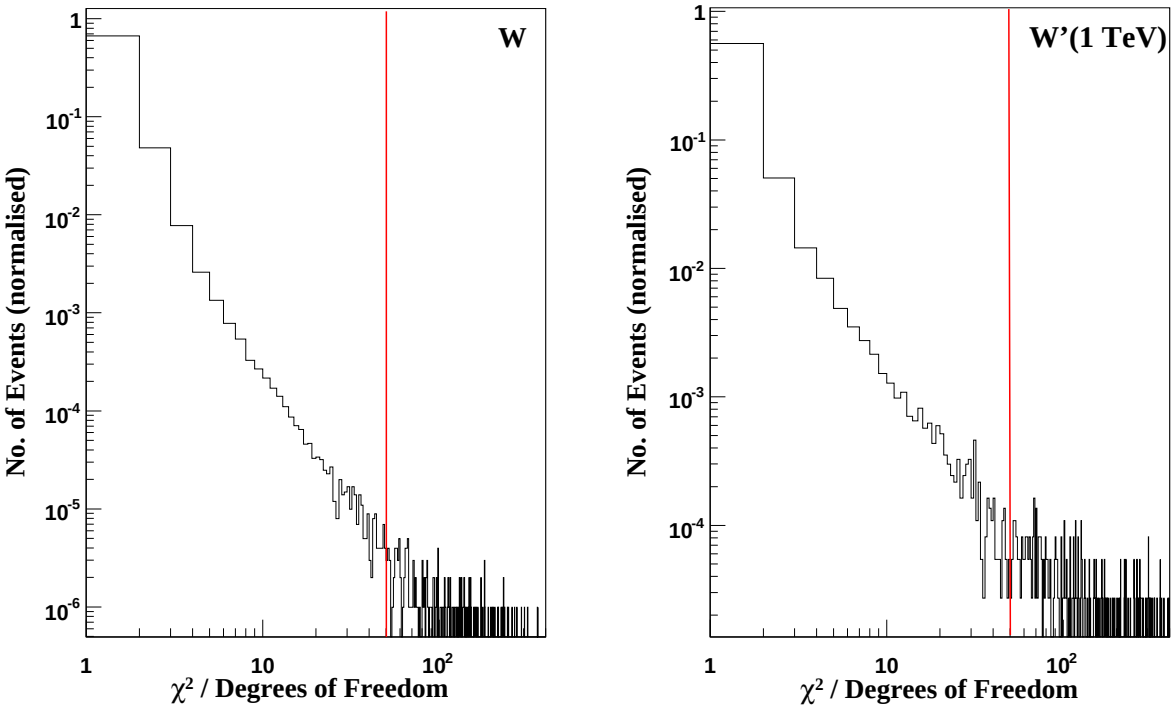

Figure 7: Normalized distribution of the χ^2 of the muon track fit divided by the degrees of freedom used within the fit for the W and the 1 TeV W' boson. Due to the larger momentum and increased bremsstrahlung probability of TeV-muons the relative fraction of excluded muons is larger in the W' boson sample.

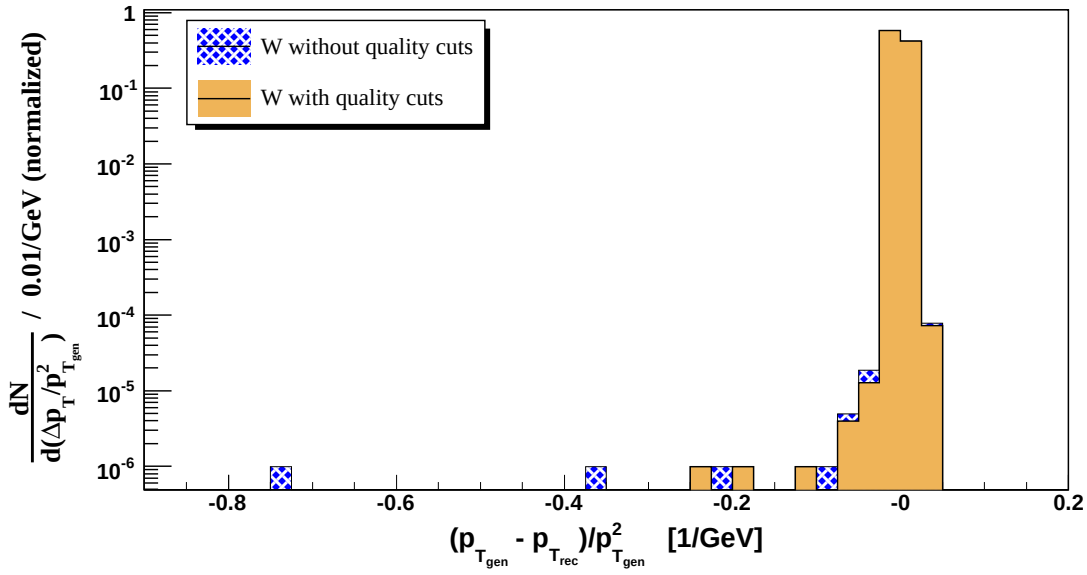

Figure 8: Effect of the χ^2 cut on the muon momentum resolution. Especially muons, whose momenta have been reconstructed with a huge discrepancy compared to the generator momenta, are excluded.

5.2.2 Single Muon Cut

$W' \to \mu\nu$ events are likely to contain only a single muon. Further muons can only arise from underlying events or pile-up. Since the underlying events are mainly lost through the beam pipe, mostly muons from additional proton-proton reactions may yield background. The pile-up events are mainly QCD events containing jets and thus have a large fraction of hadronic particles, but contain only a small number of muons. The signal events with a second global reconstructed muon are less than 3%.

Z bosons decaying into leptons, produce, in contrast to the W and W' bosons, always lepton pairs. Since the highest energy muon originating from a Z combined with the naturally comprising missing transverse energy at pp-colliders gives rise to large transverse invariant masses, it poses background in the region above $M_{\mathrm{T}} > 200\ \mathrm{GeV}$. To exclude this background the events are required to contain only one global reconstructed muon.

5.2.3 Muon Isolation

Muons from the decay of W' bosons are isolated in contrast to muons arising from the decay chain within a jet, *i.e.* no other particles are flying in the same direction as the muon. Only underlying events and pile-up might produce particles casually flying in the muon direction.

As described in detail in [19] different muon isolation algorithms are implemented in the CMS reconstruction software, all based on the same principle: in a cone with a radius $\Delta R = \sqrt{(\Delta\eta)^2 + (\Delta\phi)^2}$ around the muon direction the transverse energy deposit or the transverse momentum excluding the muon itself is measured within some detector component.

For the calorimeter isolation the transverse energy deposit inside a cone is computed within the calorimeters, while for the pixel and the tracker isolation the p_{T} of the particles in this cone is measured. All three algorithms have been tested with some variations of the parameters. The tracker isolation with the default value (ΔR = 0.17), which has already been optimised using a $W \to \mu\nu$ sample [19], gives the best results and is therefore used for this feasibility study. The calorimeter isolation algorithm has the drawback that its quality depends on the amount of underlying events and becomes less efficient at high luminosities. While the pixel algorithm relies on the local track reconstruction using at most three layers of the pixel detector, the small lever arm limits a reasonable reconstruction to tracks with a p_{T} larger 10 GeV (for details see [17] or [19]). Since the tracker isolation algorithm relies on the tracker, a robust and high quality reconstruction using several silicon layers is guaranteed and thus a good basis for track isolation is provided. Only tracks originating from the same collision vertex as the muon are used to calculate the transverse momentum within the cone, so that this algorithm is less sensitive to pile-up than the calorimeter isolation. In addition only tracks with a p_{T} larger than 0.8 GeV are reconstructed to improve the efficiency of the algorithm.

In figure 9 the distribution of the transverse momentum within the isolation cone is shown for background and signal according to a luminosity of 10 fb^{-1}. The cut at 0.8 GeV on this variable has been determined by optimizing signal efficiency times purity as a function of the isolation value. Since the algorithm only reconstructs tracks with p_{T} larger 0.8 GeV within the isolation cone, the cut is identical to the requirement of having no additional tracks within the cone around the muon.

5.3 Distributions of Characteristic Quantities

After applying all stated selection cuts, the characteristic variables are shown for signal and background for an integrated luminosity of 10 fb^{-1}. Tables 3 and 4 give an overview of the number of events in 10 fb^{-1} which survive the cuts. The efficiency is given with respect to the number of events after the preselection.

5.3.1 Transverse Momentum of the Muon

In figure 10 the p_{T}-distribution of the 1 TeV and 5 TeV W' boson signal and the background are shown. The muons arising from background processes dominate the momentum distribution at low momenta, but their contribution rapidly falls with larger momenta. Over the whole p_{T}-range the fraction of $W \to \mu\nu$ represents the largest background. This justifies that for large transverse invariant masses only the $W \to \mu\nu$ background has been taken into account.

The spikes at large momenta arise from single muons, which have been reconstructed with a too large momentum. Because of the limited number of detector-simulated events, which is smaller than the number of events expected in 10 fb^{-1}, the background has to be scaled to the one expected in 10 fb^{-1}.

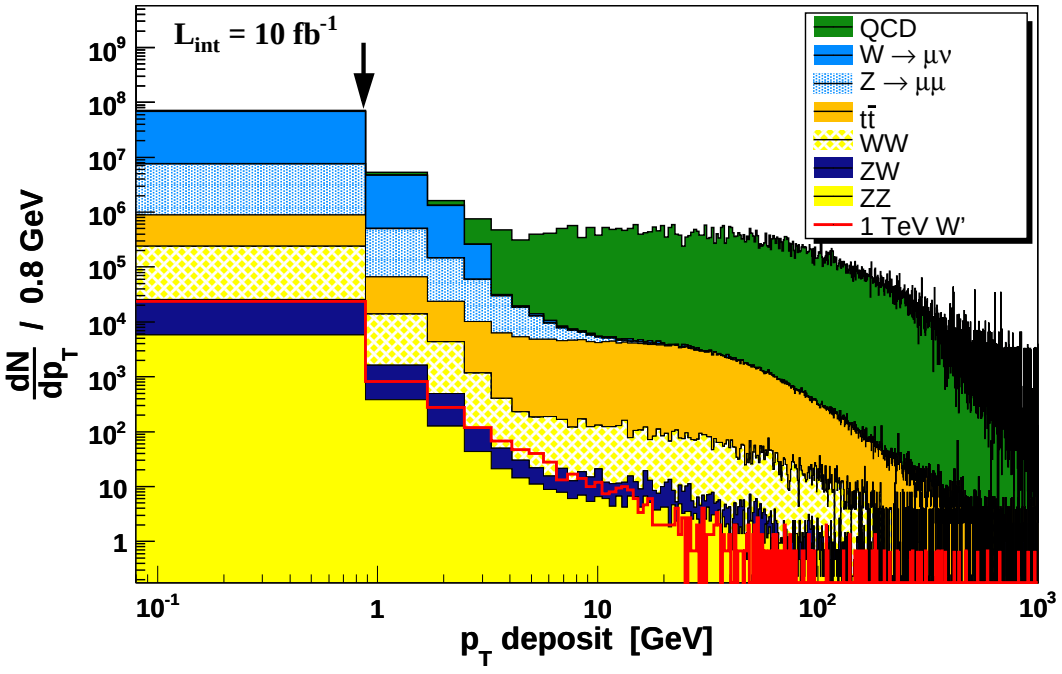

Figure 9: Transverse momentum in a cone around the muon as a result of the tracker isolation algorithm. Signal efficiency times purity has been optimised to obtain the cut (arrow).

Events in 10 fb^{-1} (Signal, $W' \to \mu\nu$ and W)					
Cut	1 TeV	3 TeV	5 TeV	7 TeV	$W \to \mu\nu$
Total	$3.01{\cdot}10^{4}$	$1.61{\cdot}10^{2}$	$2.73{\cdot}10^{0}$	$3.70{\cdot}10^{-2}$	$9.84{\cdot}10^{7}$
Preselection	$2.45{\cdot}10^{4}$	$1.35{\cdot}10^{2}$	$2.33{\cdot}10^{0}$	$3.13{\cdot}10^{-2}$	$6.73{\cdot}10^{7}$
μ-Quality	$2.42{\cdot}10^{4}$	$1.31{\cdot}10^{2}$	$2.24{\cdot}10^{0}$	$2.97{\cdot}10^{-2}$	$6.71{\cdot}10^{7}$
Single μ	$2.38{\cdot}10^{4}$	$1.27{\cdot}10^{2}$	$2.19{\cdot}10^{0}$	$2.96{\cdot}10^{-2}$	$6.61{\cdot}10^{7}$
μ-isolation	$2.22{\cdot}10^{4}$	$1.19{\cdot}10^{2}$	$2.06{\cdot}10^{0}$	$2.88{\cdot}10^{-2}$	$6.11{\cdot}10^{7}$
Efficiency	90.7%	88.4%	88.5%	91.8%	90.8%

Table 3: W' signal events and W background events remaining after the subsequent application of the selection cuts as described in section 5.1 and 5.2.

Events in 10 fb^{-1} (Background)						
Cut	$Z \to \mu\mu$	QCD	tt̄	WW	ZW	ZZ
Total	$7.83{\cdot}10^{6}$	$6.90{\cdot}10^{9}$	$1.88{\cdot}10^{6}$	$2.69{\cdot}10^{5}$	$1.11{\cdot}10^{5}$	$1.11{\cdot}10^{4}$
Preselection	$7.46{\cdot}10^{6}$	$5.10{\cdot}10^{7}$	$9.84{\cdot}10^{5}$	$2.42{\cdot}10^{5}$	$2.20{\cdot}10^{4}$	$6.64{\cdot}10^{3}$
μ-Quality	$7.42{\cdot}10^{6}$	$5.00{\cdot}10^{7}$	$9.75{\cdot}10^{5}$	$2.41{\cdot}10^{5}$	$2.19{\cdot}10^{4}$	$6.60{\cdot}10^{3}$
Single μ	$4.00{\cdot}10^{5}$	$4.44{\cdot}10^{7}$	$7.05{\cdot}10^{5}$	$2.16{\cdot}10^{5}$	$1.60{\cdot}10^{4}$	$2.00{\cdot}10^{3}$
μ-isolation	$3.65{\cdot}10^{5}$	$1.29{\cdot}10^{6}$	$4.58{\cdot}10^{5}$	$1.93{\cdot}10^{5}$	$1.45{\cdot}10^{4}$	$1.62{\cdot}10^{3}$
Efficiency	4.9%	$1.8{\cdot}10^{-4}$	46.5%	79.8%	65.9%	24.4%

Table 4: Background events, which remain after the subsequent application of the selection cuts.

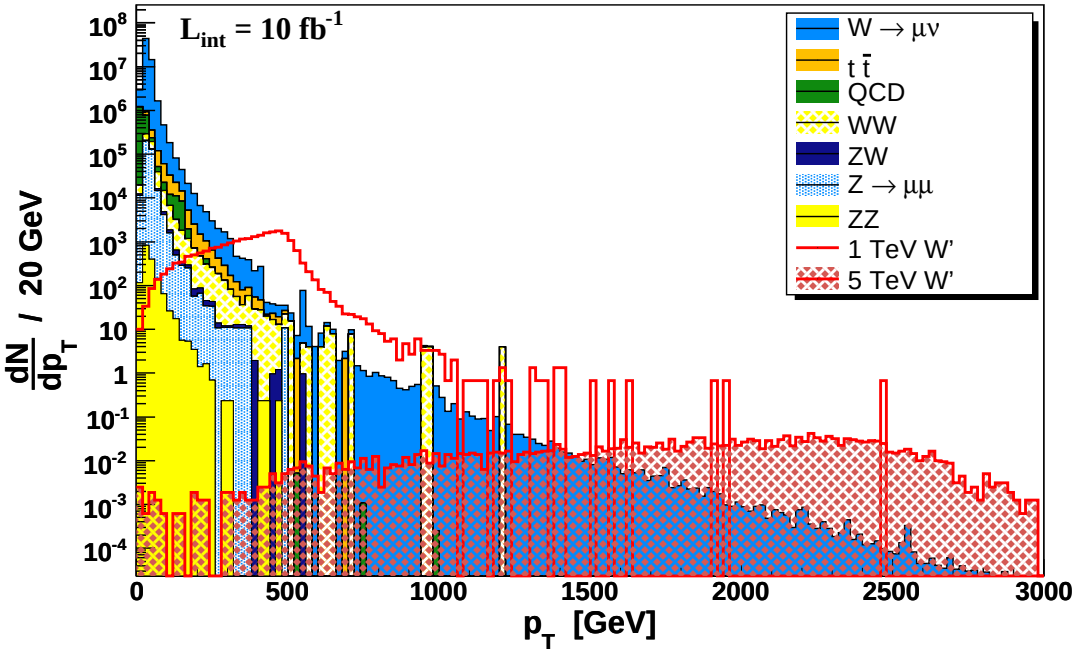

Figure 10: Signal (1 TeV and 5 TeV W', non-stacked) and background (stacked) distribution of the transverse momentum of the highest energy muon. The background is rapidly decreasing with large momenta, while the signal shows a Jacobian peak, which is smeared out due to the detector resolution.

The 1 TeV signal distribution is hidden by the huge background at momenta smaller than 300 GeV. But a Jacobian peak, much larger then the expected background, is clearly visible around $M_{W'}/2$. The peak is smeared out due to the detector resolution.

The p_T-distribution of the 5 TeV signal is distributed over a range up to 3 TeV, but still a Jacobian peak is visible. For transverse momenta above 1500 GeV, the 5 TeV W' boson signal exceeds the background. However, the expected number of signal events within an integrated luminosity of 10 fb^{-1} is less than 5 for a 5 TeV W' boson and thus the discovery of such a heavy object is only possible with a large amount of data.

For masses between 1–5 TeV the Jacobian peak, located at $M_{W'}/2$, is smeared out more and more because of the detector resolution. As shown in figure 1 the expected number of W' boson events decreases rapidly with the assumed W' boson mass.

5.3.2 Missing Transverse Energy

The missing transverse energy is calculated by summing up all energy deposits in the calorimeter towers (ECAL + HCAL), which are weighted according to their angular direction seen from the vertex. Since the muons deposit only a small fraction of their energy within the calorimeter, the energy imbalance in the transverse plane caused by the muons has to be corrected. The missing transverse energy distribution after the application of all selection criteria is shown in figure 11 for the 1 TeV and 5 TeV signal (non-stacked) and the background (stacked).

The distribution, especially in the signal region above 200 GeV, is almost identical to the muon p_T-distribution. This is evident, since the large amount of missing transverse energy is not given by calorimeter deposits, but by the large momentum of the muon, which deposits only a very small amount of its energy in the calorimeters. Roughly speaking, the missing transverse energy is given by the transverse muon momentum smeared by the calorimeter deposits.

5.3.3 Angle between Muon and Missing Transverse Energy

Since the missing energy can only be determined in the transverse plane at a pp-collider, the angle between the muon and the missing energy is measured in this plane. The distribution is shown in figure 12. While for most backgrounds (QCD, $t\bar{t}$, ZZ) this variable is uniformly distributed, it peaks for W, Z and especially for the signal at 180°. For the W and W' bosons this behaviour is given by the decay properties: in the rest frame of the

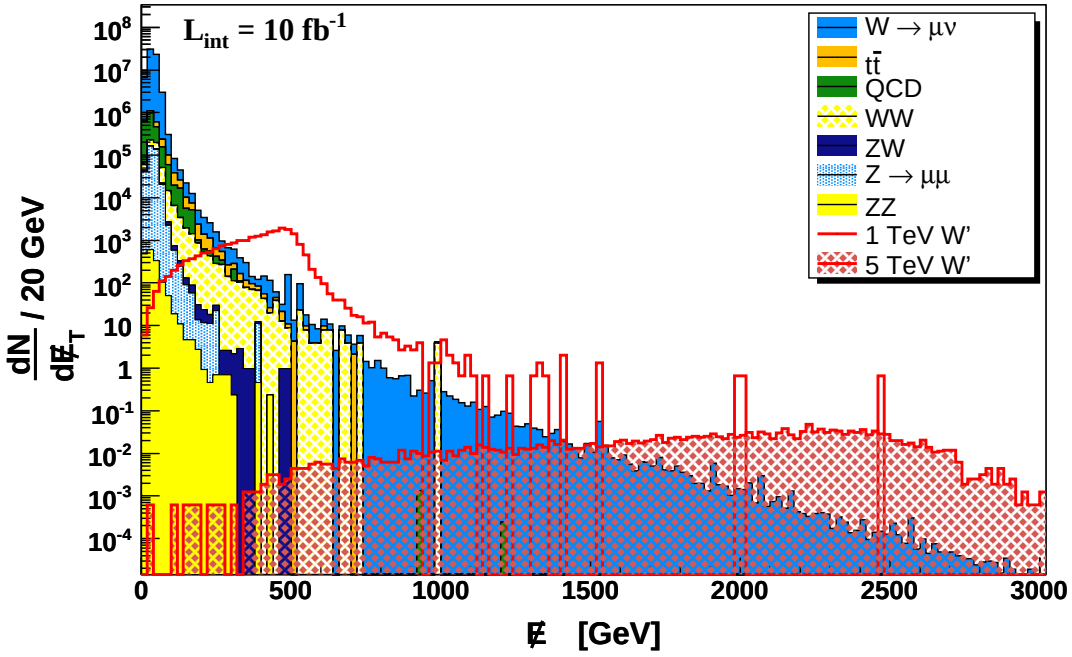

Figure 11: Missing energy in the transverse plane for the signal (1 TeV and 5 TeV W', non-stacked) and the stacked background. For large missing energies the distribution is determined by the missing energy produced by the large transverse momentum carried by the muon and not by calorimeter deposits.

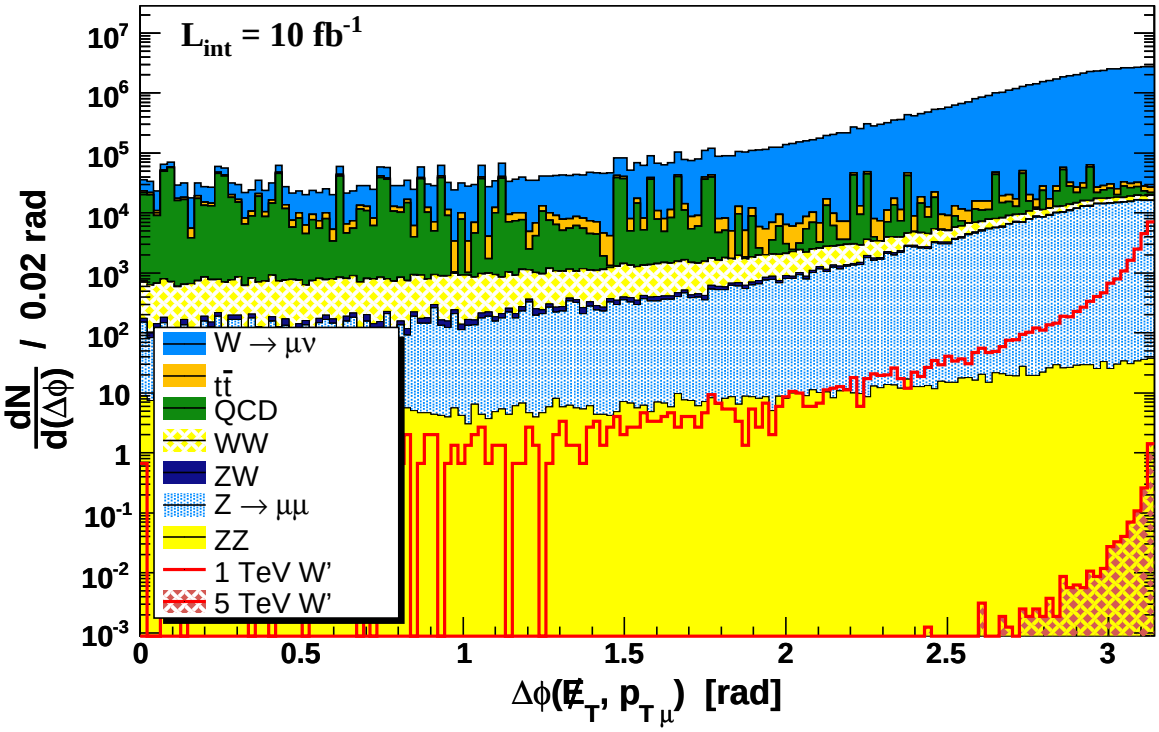

Figure 12: Distribution (stacked background and non-stacked signal) of the angle between the transverse missing energy and the transverse momentum of the muon in the transverse plane. The signal strongly peaks at 180°.

W/W' boson the muon and neutrino are emitted back-to-back. The angle in the transverse plane changes only due to transverse momenta of the W/W' boson. Due to the smaller muon and neutrino p_{T} in case of a W boson compared to ones from a W' boson, boosts have a larger impact on the angle in case of a W.

The $Z \to \mu\mu$ events also have an accumulation around 180° due to the event selection and detector inefficiencies. Demanding only single muon events, one muon has to escape undetected. This causes an energy imbalance in the direction of the undetected muon, faking missing energy. As a result one obtains a W-like signature of a muon accompanied by missing energy in the opposite direction.

5.3.4 Transverse Invariant Mass

Finally these three variables, the transverse momentum of the muon, the missing transverse energy and the angle between both in the transverse plane are combined to the transverse invariant mass using the formula

$$M_{\mathrm{T}} = \sqrt{2 p_{\mathrm{T}_\mu} \not{E}_{\mathrm{T}} (1 - \cos \Delta\phi_{\mu \not{E}_{\mathrm{T}}})}. \tag{3}$$

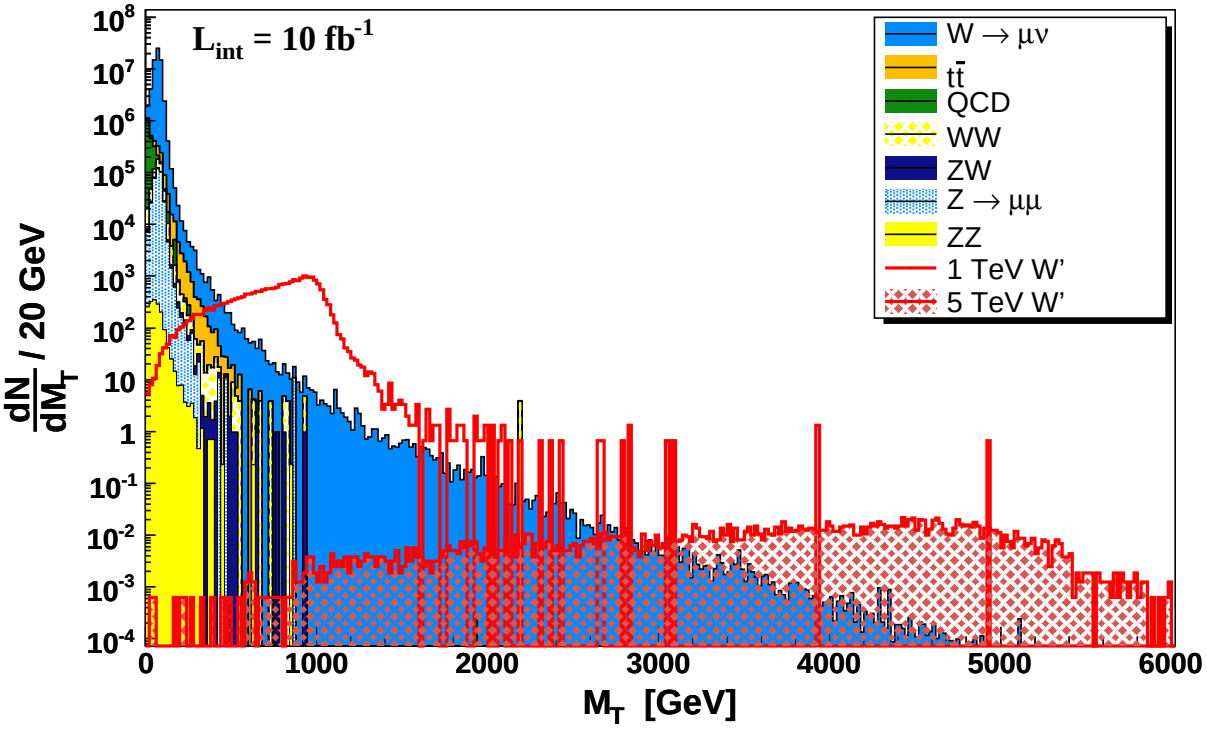

Figure 13: Signal (1 TeV and 5 TeV W') and background distribution of the transverse invariant mass.

The already observed shapes in the p_{T}- and $\not{E}_{\mathrm{T}}$-spectrum are visible and the separation of signal and background is even better (see figure 13). The background, mainly given by the $W \to \mu\nu$ sample, is exceeded by all considered W' masses for large transverse masses.

However, the question remains up to which W' mass a significant separation of signal and background is possible with a certain integrated luminosity. To obtain an answer, this distribution is used as an input to a significance test.

6 Statistical Interpretation

The transverse invariant mass spectrum is investigated in a statistical manner to decide up to which W' mass a signal for new physics can be detected if present or excluded if absent. This hypothesis test is performed using the $\mathrm{CL_S}$-method [20–22]. It interprets each of the N bins of figure 13 as a result of N independent Poisson counting experiments with the probability distribution

$$P(\mu; n) = \frac{\mu^n}{n!} \cdot e^{-\mu}. \tag{4}$$

$P(\mu; n)$ reflects the probability to obtain the result n in a counting experiment if μ is expected.

In the context of a feasibility study one can think of two different "per bin counting experiments". One counting experiment uses as mean value μ the number of *signal plus background* events ($\mu = s + b$), while the other experiment takes only the number of background events ($\mu = b$) as mean.

These two probabilities, P ($\mu = s + b; n$) and P ($\mu = b; n$), can be used to construct a discrimination variable for the significance of a signal. The Neyman-Pearson lemma ([23], proof in [24]) states that using the likelihood ratio Q_i, calculated for each bin i,

$$Q_i(m_{W'}) = \frac{P(\mu = s_i(m_{W'}) + b_i;\ n_i)}{P(\mu = b_i;\ n_i)} \tag{5}$$

minimizes errors of the first and second kind. $s_i(m_{W'})$ is the number of signal events in bin i, which is a function of the W' mass $m_{W'}$, and b_i is the number of background events in bin i. Combining all N "per bin counting experiments" for a chosen W' mass $m_{W'}$ one ends up with

$$-2\ln Q(m_{W'}) = -2\sum_{i=1}^{N}\left[n_i \ln\left(1 + \frac{s_i}{b_i}\right) - s_i\right] = 2s_{\text{tot}} - 2\sum_{i=1}^{N} n_i \ln\left(1 + \frac{s_i}{b_i}\right). \tag{6}$$

The determination of the signal significance is performed by generating numerous so called "pseudo-experiments": for each bin[2)] in the transverse invariant mass, Poisson distributed random numbers are generated once using the mean value $\mu = s_i + b_i$ and once $\mu = b_i$ to generate different n_i (see equation (6)). The resulting transverse invariant mass distribution is within statistical considerations equal to the obtained Monte Carlo distribution, *i.e.* one can interpret this as the result of an identical experiment also measuring the transverse invariant mass distribution.

This generation of "pseudo-experiments" is repeated numerously and the $-2\ln Q$ using formula (6) is calculated for each experiment. As a result one obtains two Gaussian shaped distributions for each W' mass centered at the $-2\ln Q$ of the *signal plus background* expectation and the *background only* expectation, respectively (similar to figure 14).

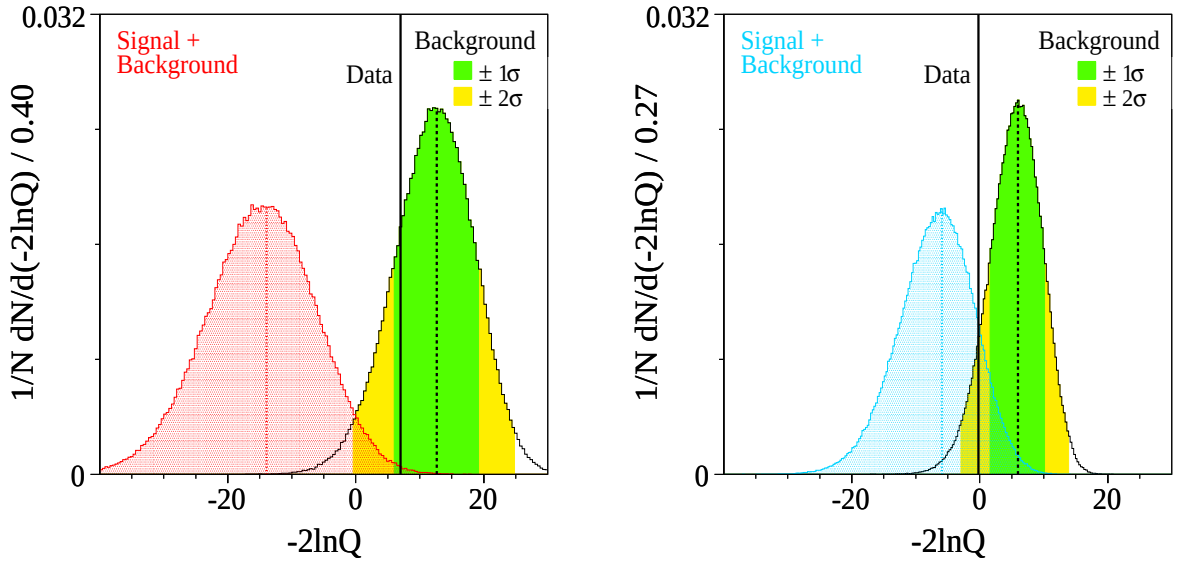

Figure 14: Perfect example of the $-2\ln Q$ distributions for two different scenarios. For the Gaussian-like distributions the corresponding σ-bands are shown: 68% (95%) of the pseudo-experiments are within one (two) standard deviations around the mean.

For the determination of the different confidence level (CL) for each hypothesis, the distributions of the achieved pseudo-statistic are integral-normalised and defined as $\mathcal{P}_{\text{s+b}}(x)$ and $\mathcal{P}_{\text{b}}(x)$ using $x := -2\ln Q$, respectively. To decide, if the hypothesis of having measured *background only* is true, the integral

$$\text{CL}_{\text{b}} = \int_{X_0}^{\infty} \mathcal{P}_{\text{b}}(x)dx \tag{7}$$

[2)] Bins with a signal to background ratio lower than 5% are neglected. The inclusion of these bins improves the sensitivity, but the systematic error introduced at the same time spoils this improvement [25].

is investigated. The integration border X_0 is the value of $-2\ln Q$ from an experiment (real data) or from Monte Carlo simulation. The calculation of the $\mathrm{CL_b}$ gives a measure in how far the experimental data are in coincidence with the *background only* expectation.

In the same manner one can test the significance for having an excess of signal above the background, using

$$\mathrm{CL_{s+b}} = \int_{X_0}^{\infty} \mathcal{P}_{\mathrm{s+b}}(x)dx. \tag{8}$$

Assuming a Gaussian character for both $\mathcal{P}_{\mathrm{s+b}}(x)$ and $\mathcal{P}_{\mathrm{b}}(x)$ a discovery is claimed if the signal plus background expectation exceeds the background only expectation by more than 5σ[3]:

$$1 - \mathrm{CL_b} \leq 2.85 \cdot 10^{-7}. \tag{9}$$

If a discovery is not possible an exclusion limit can be calculated with 95% confidence. Per convention this is mathematically given by

$$\mathrm{CL_s} := \frac{\mathrm{CL_{s+b}}}{\mathrm{CL_b}} < 0.05. \tag{10}$$

The statistical error for the confidence levels can be extracted from the σ-bands of $\mathcal{P}_{\mathrm{s+b}}(x)$ and $\mathcal{P}_{\mathrm{b}}(x)$ by changing the integration border $\mathrm{X_0}$ within the CL integrals.

7 Results

The likelihood ratio for the different W' masses (1–8 TeV) and for the Standard Model background can be calculated according to equation (6). Figure 15 shows the result of the calculations for the different investigated W' masses. It represents the $-2\ln Q$ mean values of the $\mathcal{P}_{\mathrm{b}}$ (*background only*) and $\mathcal{P}_{\mathrm{s+b}}$ (*signal plus background*) (see figure 14) as a function of the W' mass. The plot shows how well both hypotheses, *background only* and *signal plus background*, can be separated for masses below $5\ \mathrm{TeV}$.

7.1 Discovery

Based on the calculated likelihood ratio the significance for the *background only* hypothesis given by $\mathrm{CL_b}$ can be determined. As explained above the $\mathrm{CL_b}$ is a measure for the probability of having measured only background. By definition, the $\mathrm{CL_b}$ for *background only* (and therefore also the 1 - $\mathrm{CL_b}$) is identical to 0.5 (see equation (7)). This statement is validated by figure 16. The $\mathrm{CL_b}$ value for *signal plus background* is larger than 0.5 and reflects the fact that the hypothesis contains "more than only background", *i.e.* additional signal.

For a significant discrimination between the *signal plus background* and the *background only* distribution, the $\mathrm{CL_b}$ has to be close to 1. Therefore, $1 - \mathrm{CL_b}$ is used for the determination of the signal significance. In figure 16 the $1 - \mathrm{CL_b}$ for *background only* (black dotted) and the σ-bands, which state the significance of a deviation, are plotted.

According to relation (9) a discovery is claimed if a 5σ deviation from *background only* appears. Since the likelihood method investigates one-sided deviations a 5σ deviation equals $1 - \mathrm{CL_b} < 2.85 \cdot 10^{-7}$.

Figure 16 states that for an integrated luminosity of 10 fb^{-1} an expected W' boson with a mass up to 4.6 TeV can be discovered. For larger W' masses the *signal plus background* curve converges against the *background only* expectation. However, for a 8 TeV W' boson and a luminosity of 10 fb^{-1} a deviation of more than 1σ is still observable.

7.2 Exclusion

In case of no signs for new heavy charged gauge bosons, a 95% CL exclusion limit can be set. This limit corresponds to a $\mathrm{CL_s}$ less than 5%. The $\mathrm{CL_s}$ distribution for an integrated luminosity of 10 fb^{-1} as a function of the W' mass is shown in figure 17. A limit of

$$m_{W'} > 4.71\ \mathrm{TeV} \qquad \text{at 95\% CL}$$

can be set. The statistical errors are given by the $\pm 1\sigma$- and $\pm 2\sigma$-bands.

[3] One-sided 5σ deviation.

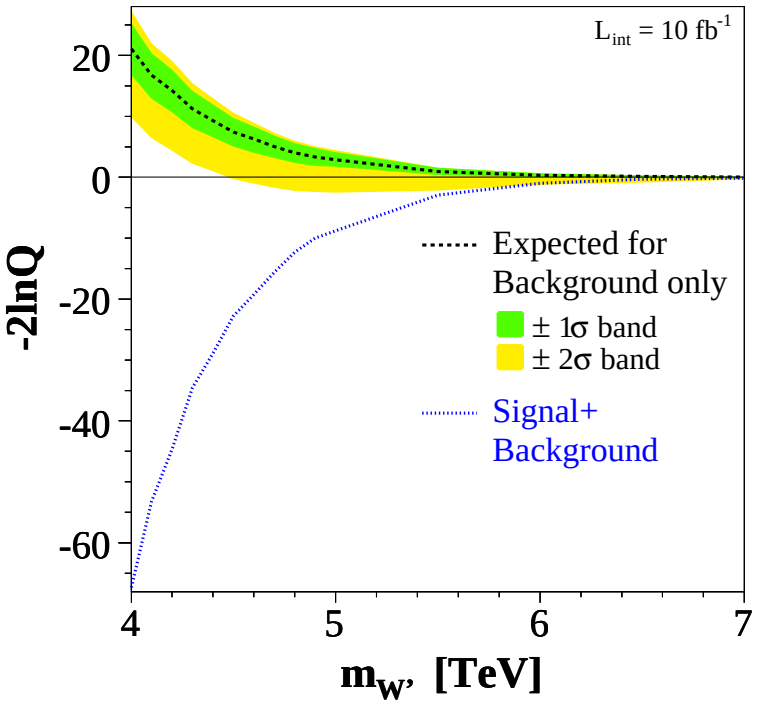

Figure 15: $-2\ln Q$ distribution for *signal plus background* and *background only* as a function of the W' mass. For the *background only* graph also the $\pm 1\sigma$ and $\pm 2\sigma$-bands are plotted. Both curves are well separated for masses below 5 TeV.

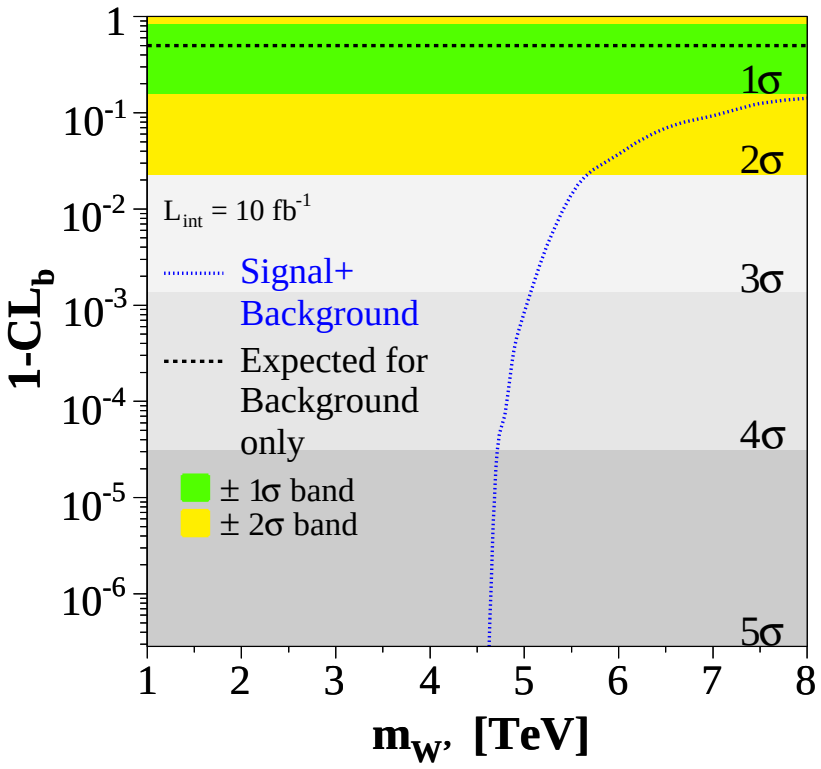

Figure 16: $1-\mathrm{CL_b}$ distribution for *signal plus background* and *background only*. By definition the *background only* curve is independent from the tested W' mass at 0.5. According to the σ-deviation of the *signal plus background* curve from the background the discovery limit is determined to be $m_{W'} = 4.6$ TeV.

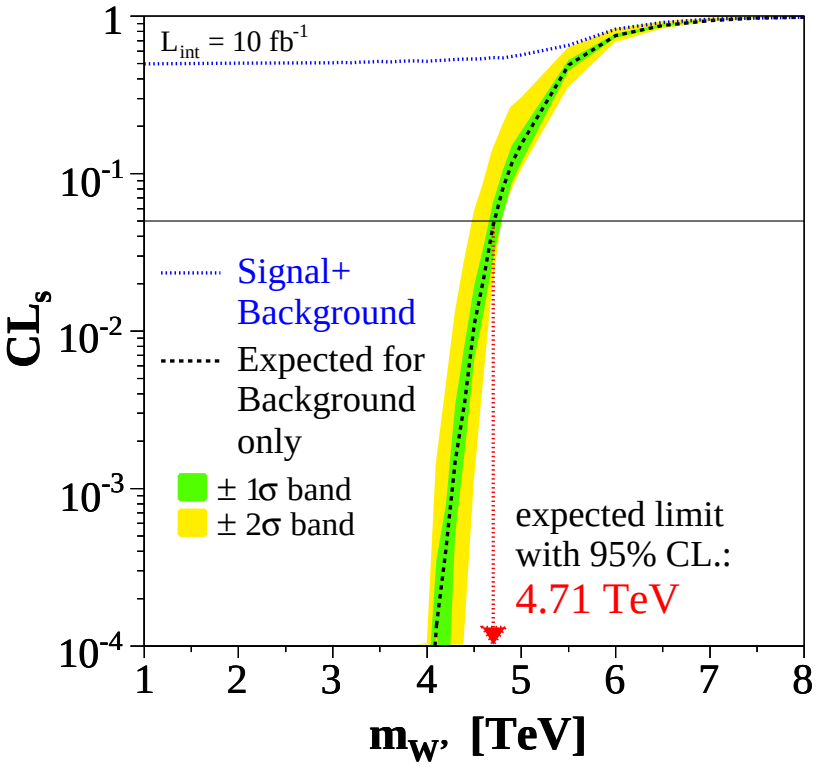

Figure 17: CL_s distribution for *signal plus background* and *background only*. For an integrated luminosity of 10 fb^{-1} the exclusion limit at 95% CL (CL_s = 0.05) is $m_{W'}$ = 4.71 TeV.

7.3 Luminosity Dependence of the Limit

In order to investigate the limit improvement the statistical method is repeated using a scaled integrated luminosity in the range 1–300 fb^{-1}. Within this luminosity range the discovery limit (see figure 18) and the 95% exclusion limit (see figure 19) are calculated for various luminosities with the corresponding statistical errors.

Already with an integrated luminosity of 1 fb^{-1} a W' boson with a mass smaller than 3.5 TeV can either be discovered or excluded with 95% CL. Including more data, the discovery as well as the exclusion limit increase up to 6 TeV for an integrated luminosity of 300 fb^{-1}.

7.4 Signal and Background Variation

To investigate the influence of a background under- or overestimation on the exclusion limit, the background is scaled. The same procedure has been repeated with the signal to investigate the sensitivity of the limit on the variation of the signal.

Figure 20 shows the exclusion limit as a variation of the background normalised to the expected background obtained from the Monte Carlo simulation. Thus, the y-axis value equal 1 is equivalent to the MC background expectation for an integrated luminosity of 10 fb^{-1}. While scaling the background the signal cross section is kept constant. Even if the background has been underestimated by a factor 50 in this feasibility study, the upper exclusion limit drops only slightly below 4.3 TeV.

The same variation has been performed for the signal, while keeping the background identical to the MC expectation. The signal cross section, normalised to the cross section of the Reference Model, has been varied in the range 0.01–2. The former case corresponds to a 100 times lower cross section, while the latter is equal to a doubled cross section. As shown in figure 21 the 95% exclusion limit is above 4 TeV taking signal scaling factors above 0.25 into account. For smaller scaling values the exclusion limit rapidly falls to zero.

7.5 Discussion of the Results

The presented statistical method highly depends on the precise knowledge of the absolute number of background events. This implies a good understanding of the detector, since misalignment and an imperfect calibration might

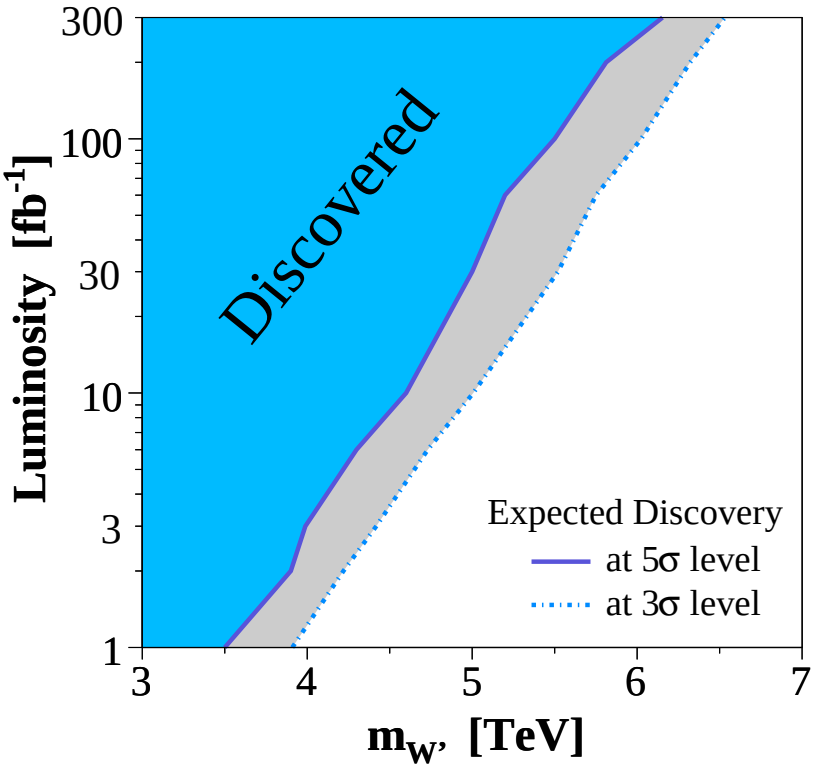

Figure 18: Discovery limit as a function of the investigated integrated luminosity. To achieve this plot the transverse invariant mass distributions for the signal and the background have been scaled to different luminosities and the discovery limit has been calculated for each distribution.

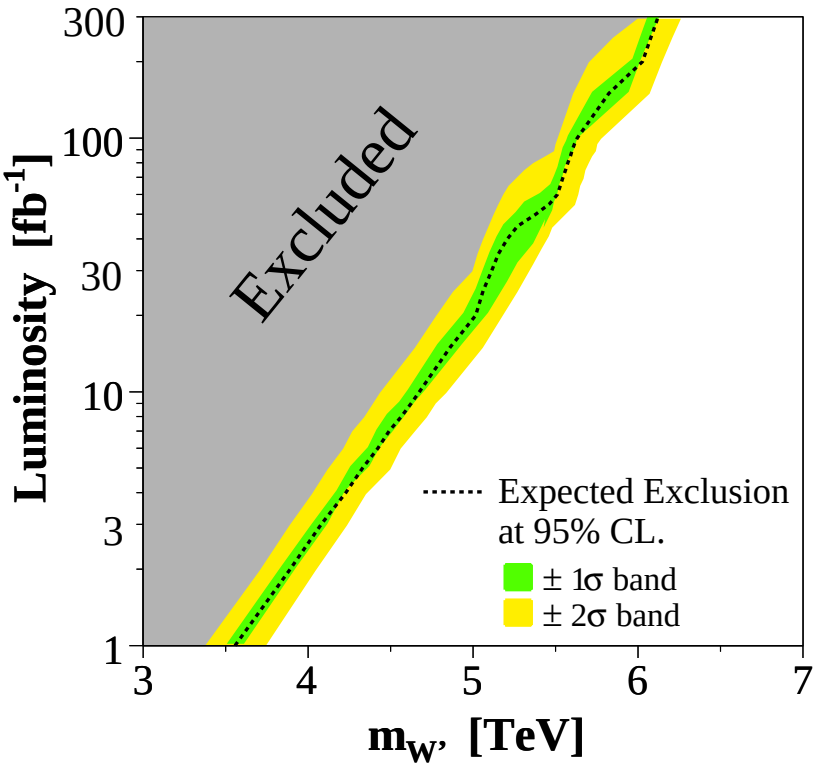

Figure 19: 95% CL exclusion limit as a function of the investigated integrated luminosity.

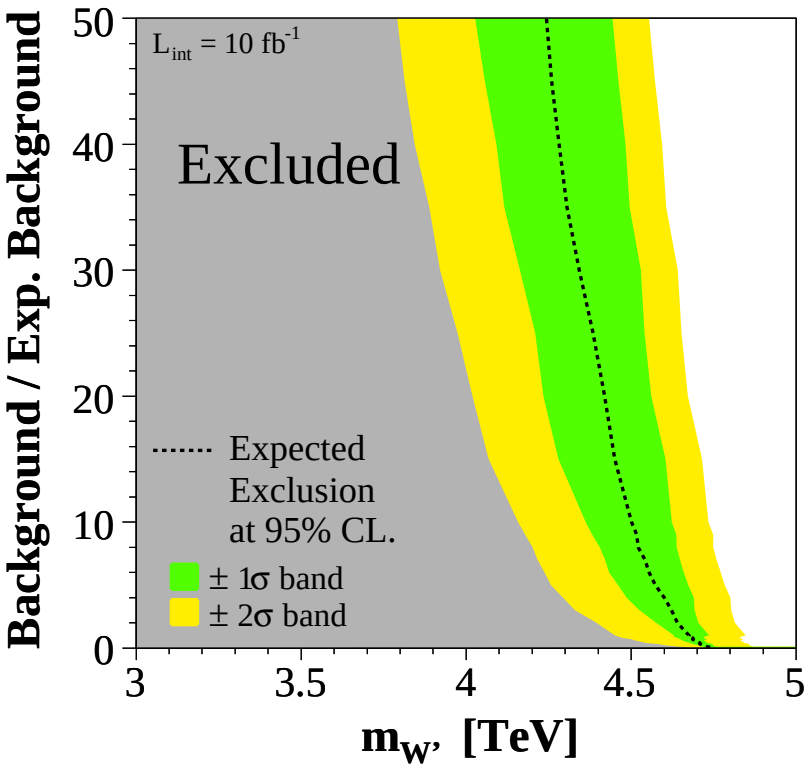

Figure 20: 95% CL exclusion limit as a variation of the expected background.

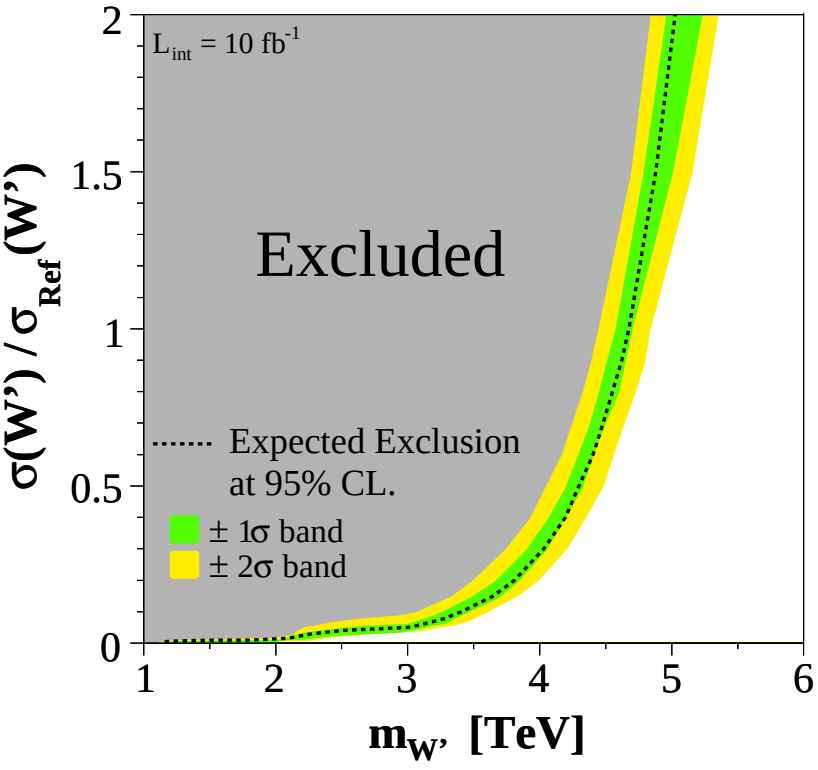

Figure 21: 95% CL limit as a variation of the expected signal.

fake additional background. One possibility to improve the knowledge of the absolute number of background events might be the analysis of the channel $W' \to e\nu$, since the momentum resolution for electrons improves with the energy. However, the electron channel might suffer from different problems (e.g. identification).

A better solution would be the use of a statistical method, which takes the difference of the signal and background shapes into account. For example a Jacobian peak and an exponential falling curve could be fitted to the signal and background, respectively. Such a fit would not be sensitive to uncertainties in the expected signal and background levels, and its result could be used to calculate the significance.

7.6 Systematic Uncertainties

Several systematical uncertainties affect the presented discovery reach for a W'. A first approach has been performed to identify the major uncertainties and to quantify them. Uncertainties may arise from imperfect theoretical knowledge such as parton density functions (PDF), higher order corrections (K-factors) or the imperfect modelling of the simulated processes. Further systematic errors arise due to an imperfect knowledge of the accelerator (luminosity) and the detector (alignment, calibration, dead detector components).

7.6.1 Theoretical Uncertainties

The current estimate of the W' mass reach depends on the accuracy of the modelling of the W' signal and the considered Standard Model backgrounds. The uncertainties arising from an imperfect knowledge of the PDFs at LHC energies and the error from the hard scale parameters have been investigated following reference [26].

The best way to evalutate theoretical uncertainties due to a certain proton PDF is to vary the errors on the parameters of the PDF fit itself. Therefore the Les Houches Accord PDFs (LHAPDF - CTEQ6.1M PDF (NLO) [28, 29]) are used to estimate the error on the cross section. The uncertainties are stated in table 5 for serveral W' masses and the main background. The cross section error rise from $\frac{\Delta\sigma}{\sigma} = {}^{+3.6\%}_{-4.3\%}$ for 1 TeV W' bosons to $\frac{\Delta\sigma}{\sigma} = {}^{+33.7\%}_{-18.9\%}$ for bosons with a mass of 5 TeV. The error on the W background is comparable with that of the W' at the corresponding invariant mass.

Hard Scale: The dependence of the observables on the choice of the Q^2 hard process scale is unphysical. Since it directly enters the parametrization of the PDFs and α_s and therefore the cross section, it provides an important contribution to the total uncertainty in the theoretical predictions. The values of Q^2 have been changed to $0.25\,\widehat{s}$ and $4.0\,\widehat{s}$ to determine the sensitivity of the cross section to the hard scale. The uncertainties are stated in table 5.

Systematic Uncertainties					
Type	1 TeV W'	2 TeV W'	3 TeV W'	4 TeV W'	5 TeV W'
PDF $\Delta\sigma/\sigma$	$^{+3.6}_{-4.3}$	$^{+6.8}_{-5.9}$	$^{+6.2}_{-8.3}$	$^{+17.1}_{-10.6}$	$^{+33.7}_{-18.9}$
Hard Scale $\Delta\sigma/\sigma$	$^{+4.1}_{-4.1}$	$^{+7.5}_{-6.9}$	$^{+10.4}_{-9.2}$	$^{+13.1}_{-10.3}$	$^{+14.8}_{-12.7}$
Luminosity $\Delta\mathcal{L}/\mathcal{L}$	$\pm 5\%$	$\pm 5\%$	$\pm 5\%$	$\pm 5\%$	$\pm 5\%$

Table 5: Systematic uncertainties arising from an imperfect theoretical knowledge (parton density functions, hard scale) and the expected luminosity error for an intergrated luminosty of 10 fb^{-1}.

7.6.2 Experimental Uncertainties

The alignment precision of the muon system limits the resolution of the muon momentum - especially for the high energetic ones. In order to study the impact of these so-called alignment uncertainties, a misalignment package is available within the CMS reconstruction framework [27]. It is possible to choose between several scenarios, which model the expected alignment uncertainties at different stages of the CMS operation.

In reference [27] it has been shown that the reconstruction performance (p_{T} resolution) for high energetic muons is only moderately influenced by a misaligned detector. However, the steep falling invariant mass distribution especially of the W background holds a potential danger for the detection of W' bosons: if only a small fraction of these events - say 1 out of 100000 - is reconstructed with a by far too large mass, which might result from a mismeasured muon momemtum, the detection of a W' becomes extremely difficult. Such a behavior would be visible in so called non-Gaussian tails for example in the p_{T} resolution distribution.
A high statistics W sample (1.4 million events) has been used to investigate the effect of a misaligned detector

on the muon momentum resolution. Since this study aims for an integrated luminosity of 10 fb^{-1} the according scenario, which reflects the expected alignment uncertainties has been chosen. Figure 22 shows the comparison of the muon resolution between the perfect aligned detector and the chosen misalignment scenario. Although the resolution is slightly degraded for the misalignment scenario, the tails of both distributions are almost identical.

Another experimental uncertainty is given by the error on the luminosity, which has been estimated to be at $\frac{\Delta\mathcal{L}}{\mathcal{L}} = \pm 5\%$ at an integrated luminostity of 10 fb^{-1}. Further systematic studies (neutron background, dead detector components, etc) have to be performed to achieve a complete picture of the uncertainties influencing this analysis.

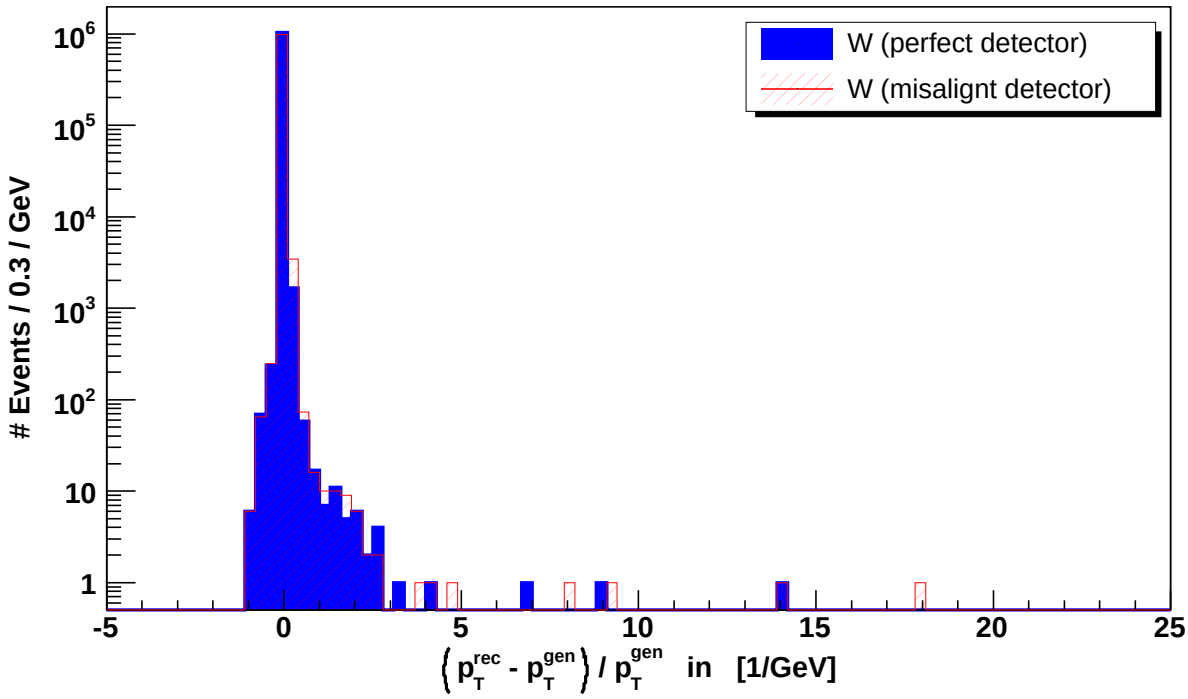

Figure 22: Comparison of the muon momentum resolution of a perfect detector with a misaligned detector. 1.4 million W events have been analysed and selection cuts have been applied (muon quality, L1 and HLT Trigger). A significant increase of events at large values is not visible within the misalignment scenario.

8 Conclusion

In this paper the first feasibility study for new heavy charged gauge bosons with the full CMS detector simulation has been presented. These new particles have been investigated within the Reference Model using the decay into a single muon plus a Standard Model neutrino. The model assumes a new heavy charged gauge boson W' to be a carbon copy of the Standard Model W, but with a different mass. The W' mass, which is the only free parameter of the Model, has been investigated in the range 1–8 TeV. All Standard Model background processes have been taken into account. According to the low luminosity phase of the LHC ($\mathcal{L} = 2 \cdot 10^{33}\ \mathrm{cm}^{-2}\,\mathrm{s}^{-1}$) on average 3.5 pile-up events have been mixed with the signal and background samples.

It has been shown that new heavy charged gauge bosons, which behave similar to the SM ones, can be discovered (5σ) with an integrated luminosity of 10 fb^{-1} with a mass up to 4.6 TeV. If no signal is visible at CMS, an exclusion limit with 95% CL of $m_{W'} > 4.71\ \mathrm{TeV}$ can be set. With an integrated luminosity of 300 fb^{-1} both limits can be extended to a W' boson mass above 6 TeV.

Variations of the signal and background cross sections have been performed to investigate the influence of an underestimation of the background or an overestimation of the signal on the expected exclusion limit. Within a wide range of variations the mass exclusion limit remains above 4 TeV for an integrated luminosity of 10 fb^{-1}. Especially the variation of the background has a rather small influence on the exclusion and discovery limit.

Systematic uncertainties resulting from parton density functions and scale dependencies have been calculated. Further studies have been performed to determine uncertainties arising from detector misalignment. These uncer-

tainties are expected to give the main contributions. However further studies are needed to obtain a full picture of the systematic uncertainties, which may have an impact on the W' discovery.

Acknowledgements

We would like to thank all the members of the CMS collaboration who contributed to the software used within this analysis and supported this study. We are grateful to J. Alcaraz, I. Belotelov, T. Cox, M. Krämer, S. Lacaprara, N. Neumeister, L. Pape, H. Pi, T. Sjostrand, M. Spiropulu, V. Valuev and M. Zöller for their discussions and assistance.

References

[1] C. Hof, *"Detection of New Heavy Charged Gauge Bosons with the Future CMS Detector"*, **Diploma Thesis at RWTH Aachen, November 2005**, *http://www.physik.rwth-aachen.de/∼hebbeker/theses/hof_diploma.ps*

[2] R. N. Mohapatra and J. C. Pati, *"Left-Right Gauge Symmetry and an 'Isoconjugate' Model of CP Violation"*, **Phys. Rev. D11 (1975) 566-571**

[3] R. N. Mohapatra and G. Senjanovic *"Neutrino Mass and Spontaneous Parity Nonconservation"*, **Phys. Rev. Lett. 44 (1980) 912**

[4] J. C. Pati and A. Salam, *"Lepton Number as the Fourth Color"*, **Phys. Rev. D10 (1974) 275-289**

[5] R. Mohapatra, *"Unification and Supersymmetry"*, **Springer Verlag (1996) Second Edition, Berlin**

[6] W. Grimus, *"Introduction to Left-Right Symmetric Models"*, **Lectures given at the 4th Hellenic School on Elementary Particle Physics, Corfu, Greece (1992)**

[7] G. Altarelli, B. Mele and M. Ruiz-Altaba, *"Searching for New Heavy Vector Bosons in $\overline{p}p$-Colliders"*, **Z. Phys. C45 (1989) 109**

[8] Z. Sullivan, *"Searching for W' Bosons at Hadron Colliders"*, **TeV4LHC Meeting (2004)**

[9] T. Han, H. E. Logan, B. McElrath, L.-T. Wang, *"Phenomenology of the Little Higgs Model"*, **Phys. Rev. D67 (2003) 095004**

[10] Z. Sullivan, *"How to Rule Out Little Higgs (and Constrain Many Other Models) at the LHC"*, **Proceedings of XXXVIIIth Rencontres de Moriond: QCD (2003), The Goi Publishers, 379**

[11] T. Affolder *et al.*, *"Search for Quark Lepton Compositeness and a Heavy W' Boson Using the $e\nu$-Channel in $\overline{p}p$-Collisions at $\sqrt{s} = 1.8$ TeV"*, **Phys. Rev. Lett. 87 (2001) 231803**

[12] P. Langacker and S. Uma Sankar, *"Bounds on the Mass of W_R and the W_L - W_R Mixing Angle ξ in General SU(2)$_L$ × SU(2)$_R$ × U(1) Models"*, **Phys. Rev. D40 (1989) 1569-1585**

[13] T. Sjostrand, L. Lonnblad and S. Mrenna, *"PYTHIA 6.2: Physics and Manual"*, **hep-ph/0108264, 2001**

[14] The CMS Collaboration, *"CMS Technical Proposal"*, **CERN/LHCC 94-38, LHCC/P1, 1994**

[15] The CMS Collaboration, *"The Muon Project - Technical Design Report"*, **CERN/LHCC 97-32, CMS TDR 4, 1997**

[16] N. Amapane *et al.*, *"Monte Carlo Simulation of Inclusive Single- and Di-Muon Samples "*, **CMS Note 2002/041**

[17] The CMS Collaboration, *"Detector Performance and Software - Technical Design Report (Volume 1)"*, **CERN/LHCC 2006-001, CMS TDR 8.1, 2006**

[18] The CMS Collaboration, *"Data Acquisition and High-Level Trigger - Technical Design Report (Volume 2)"*, **CERN/LHCC 02-26, CMS TDR 6, 2002**

[19] N. Amapane, M. Fierro and M. Konecki, *"High Level Trigger Algorithms for Muon Isolation"*, **CMS Note 2002/040**

[20] A. L. Read, *"Modified Frequentist Analysis of Search Results (The CL_s Method)"*, **Prepared for Workshop on Confidence Limits, Geneva, Switzerland (2000)**

[21] E. Gross and A. L. Read, *"Prospects for Standard Model Higgs Search in the LEP 2000 Run"*, **Proceedings of 14th Rencontres de Physique de la Valle d'Aoste: Results and Perspectives in Particle Physics, La Thuile, Valle d'Aoste, Italy (2000)**

[22] A. L. Read, *"Presentation of Search Results: The CL_s Technique"*, **J. Phys. G28 (2002) 2693-2704**

[23] G. Cowan, *"Statistical Data Analysis"*, **Oxford University Press, New York, 1998**

[24] S. Brandt, *"Statistical and Computational Methods in Data Analysis"*, **Springer, New York, 1997**

[25] A. Favara and M. Pieri, *"Optimal Statistical Analysis of Search Results"*, **L3 Internal Note 2066, 1997**

[26] P. Bartalini, R. Chierici and A. De Roeck, *"Guidelines for the estimation of theoretical uncertainties at the LHC"*, **CMS Note 2005/013**

[27] I. Belotelov *et al., "Simulation of Misalignment Scenarios for CMS Tracking Devices"*, **CMS Note 2006/008**

[28] D.R. Stump, Prepared for 31st International Conference on High Energy Physics (ICHEP 2002), Amsterdam, The Netherlands, 24-31 Jul 2002. Published in "Amsterdam 2002, ICHEP" 265-267

[29] H. Baer *et al.*, **hep-ph/0403045**, Code and documentation available at *http://durpdg.dur.ac.uk/lhapdf/*